Sphingosine-1-phosphate transporter spinster homolog 2 is essential for iron-regulated metastasis of hepatocellular carcinoma

Min Li,[1,2,8] Yuxiao Tang,[1,8] Dongyao Wang,[3,8] Xiaofeng Zhai,[4] Hui Shen,[1] Chen Zhong,[5] Man Yao,[4] Aiguo Jin,[4] Zhengjun Zhou,[6] Shaolai Zhou,[6] Jia Fan,[6] Chang-quan Ling,[4] and Chen Ling[5,7]

[1]Department of Nutrition, Faculty of Naval Medicine, Second Military Medical University, Shanghai 200433, China; [2]Institute of International Medical Science and Technology, Sanda University, Shanghai 201209, China; [3]School of Pharmacy, Second Military Medical University, Shanghai 200433, China; [4]Changhai Hospital, Second Military Medical University, Shanghai 200433, China; [5]State Key Laboratory of Genetic Engineering and Engineering Research Center of Gene Technology (Ministry of Education), School of Life Sciences, Zhongshan Hospital, Fudan University, Shanghai 200438, China; [6]Liver Surgery Department, Liver Cancer Institute, Zhongshan Hospital, Fudan University, Shanghai 200032, China; [7]Department of Clinical Laboratory, The First Affiliated Hospital of Wenzhou Medical University, Wenzhou, Zhejiang 325000, China

Iron dyshomeostasis is associated with hepatocellular carcinoma (HCC) development. However, the role of iron in HCC metastasis is unknown. This study aimed to elucidate the underlying mechanisms of iron's enhancement activity on HCC metastasis. In addition to the HCC cell lines and clinical samples *in vitro*, iron-deficient (ID) mouse models were generated using iron-free diet and transferrin receptor protein knockout, followed by administration of HCC tumors through either orthotopic or ectopic route. Clinical metastatic HCC samples showed significant ID status, accompanied by overexpression of sphingosine-1-phosphate transporter spinster homolog 2 (SPNS2). Mechanistically, ID increased SPNS2 expression, leading to HCC metastasis in both cell cultures and mouse models. ID not only altered the anti-tumor immunity, which was indicated by phenotypes of lymphatic subsets in the liver and lung of tumor-bearing mice, but also promoted HCC metastasis in a cancer cell autonomous manner through the SPNS2. Since germline knockout of globe SPNS2 showed significantly reduced HCC metastasis, we further developed hepatic-targeting recombinant adeno-associated virus vectors to knockdown SPNS2 expression and to inhibit iron-regulated HCC metastasis. Our observation indicates the role of iron in HCC pulmonary metastasis and suggests SPNS2 as a potential therapeutic target for the prevention of HCC pulmonary metastasis.

INTRODUCTION

Hepatocellular carcinoma (HCC) is one of the leading causes of cancer death worldwide, with more than 625,000 deaths annually.[1] Among these, metastasis accounts for approximately 90% of cancer-related mortality.[2] Current treatments include surgical resection, trans-arterial chemoembolization and radioembolization,[3] tyrosine kinase inhibitor Sorafenib,[4] liver transplantation,[5] combined locoregional-immunotherapy,[6] and integrative traditional therapy.[7] Unfortunately, HCC harbors highly metastatic properties, accounting for postoperative recurrence and metastasis. The underlying mechanisms remain largely unknown.

Iron is an essential nutrient that enables a variety of biological processes. Iron metabolism and solid tumor biology are intimately interconnected.[8] Excess iron produces reactive oxygen species through Fenton reaction, which may result in mutagenicity and malignant transformation. In addition, high amounts of iron are required for malignant cell proliferation.[9] Furthermore, iron has multiple regulatory effects on the immune system, affecting tumor surveillance.[10] Iron overload is a risk factor for HCC,[11] especially in patients with hereditary hemochromatosis[12] and β-thalassemia.[13] Therefore, iron chelator deferoxamine (DFO) was proposed and resulted in a 20% overall response rate in a clinical study of ten patients with advanced HCC,[14] prompting further research of combination treatment.[15] We reported that iron overload reduces hepatic-specific microRNA122 (miR122) expression,[16] a potential HCC suppressor gene.[17,18] Therefore, iron plays a role both as an initiator in an early phase of HCC, and once malignancy has occurred, as a promoter for HCC growth. In contrast, there was little research aiming to elucidate the role of iron on HCC metastasis.

Recently, a genome-wide *in vivo* screen identified that lack of sphingosine-1-phosphate (S1P) transporter spinster homolog 2 (SPNS2), either globally or in a lymphatic endothelial-specific manner, led to a higher percentage of effector T cells and natural killer cells present

Figure 1. Low iron was observed in clinical HCC samples and was potentially associated with metastasis

(A and B) Human HCC tumors (T) and their non-tumor (NT) adjacent tissues were subjected to determine (A) iron content and (B) mRNA (left) and protein (right) expression of iron-related genes. N = 29. (C) Iron content in the human normal (N) liver tissues, NT adjacent tissues, and HCC tumors was determined by magnetic resonance imaging. Both representative (left) and quantitative data (right) were showed. Red arrow, tumor. N = 10. (D) Human HCC tumors were resected from patients with metastasis (M) or non-metastasis (NM) 5 year later. Both iron content (left) and the mRNA expression (right) of iron-related genes were determined. N = 15. (E) The mRNA reads of TFRC, HAMP, and FTL from The Cancer Genome Atlas (TCGA) database. Data from a total of 374 primary solid T samples and 50 adjacent NT samples was analyzed. (F) The Kaplan-Meier analysis of overall survival for TFRC and HAMP subpanels of HCC patients from the TCGA database. N = 371. Data were presented as mean ± SEM. *p < 0.05, **p < 0.01 versus NT or versus NM. HCC, hepatocellular carcinoma; TFRC, transferrin receptor; HAMP, hepcidin; FTL, ferritin light chain.

in the lung. This allowed for potent tumor cell killing and an overall decreased metastatic burden.[19] It was suggested that targeting SPNS2 is potentially a more promising option for regulating metastatic colonization than existing S1P pathway modulators.[20] However, the roles of hepatic SPNS2 and the outcome of SPNS2 overexpression had never been elucidated during cancer metastasis.

In this manuscript, we first report that iron deficiency (ID) is a risk factor for HCC metastasis in patients and is associated with poor prognosis with shorter overall survival. ID led to HCC metastasis in various *in vitro* and *in vivo* models. Mechanistically, hepatic SPNS2 is a key regulator during the ID-induced HCC pulmonary metastasis. In addition, our efforts to develop hepatic-targeting recombinant adeno-associated virus (AAV) vectors to knockdown SPNS2 expression provide a new therapeutic target for the treatment of iron-regulated HCC metastasis.

RESULTS
Lower iron content is associated with clinical HCC samples
In the first set of experiments, tumor (T) samples and adjacent non-tumor (NT) tissues were resected from 29 HCC patients.

The results of iron content assay indicated that tumors had lower iron (Figure 1A). In addition, the tumor tissues presented higher transferrin receptor (TFRC) expression, as well as lower hepcidin (HAMP) and ferritin light chain (FTL) expression, suggesting their status of low iron (Figure 1B). Furthermore, the results of magnetic resonance imaging (N = 10) indicated that normal (N) and adjacent NT tissues had similar levels of iron, while tumor tissues had a lower level (Figure 1C). In the second set of experiments, we obtained additional 15 HCC tissues from patients who had metastasis (M) 5 years later, mostly in the lung, and another 15 HCC tissues from age-paired patients who had non metastasis (NM). The iron content and TFRC expression in the tumor with metastasis was significantly lower and higher than that with NM, respectively (Figure 1D). These corroborated the ID statues in the group with metastasis.

Next, HCC RNA sequencing (RNA-seq) data were retrieved from the public TCGA database (https://portal.gdc.cancer.gov/). As shown in Figure 1E, there is significant difference in the level of iron-related genes, TFRC and HAMP, between tumor tissues (N = 374) and adjacent NT liver tissues (N = 50). We also analyzed the 50 adjacent NT
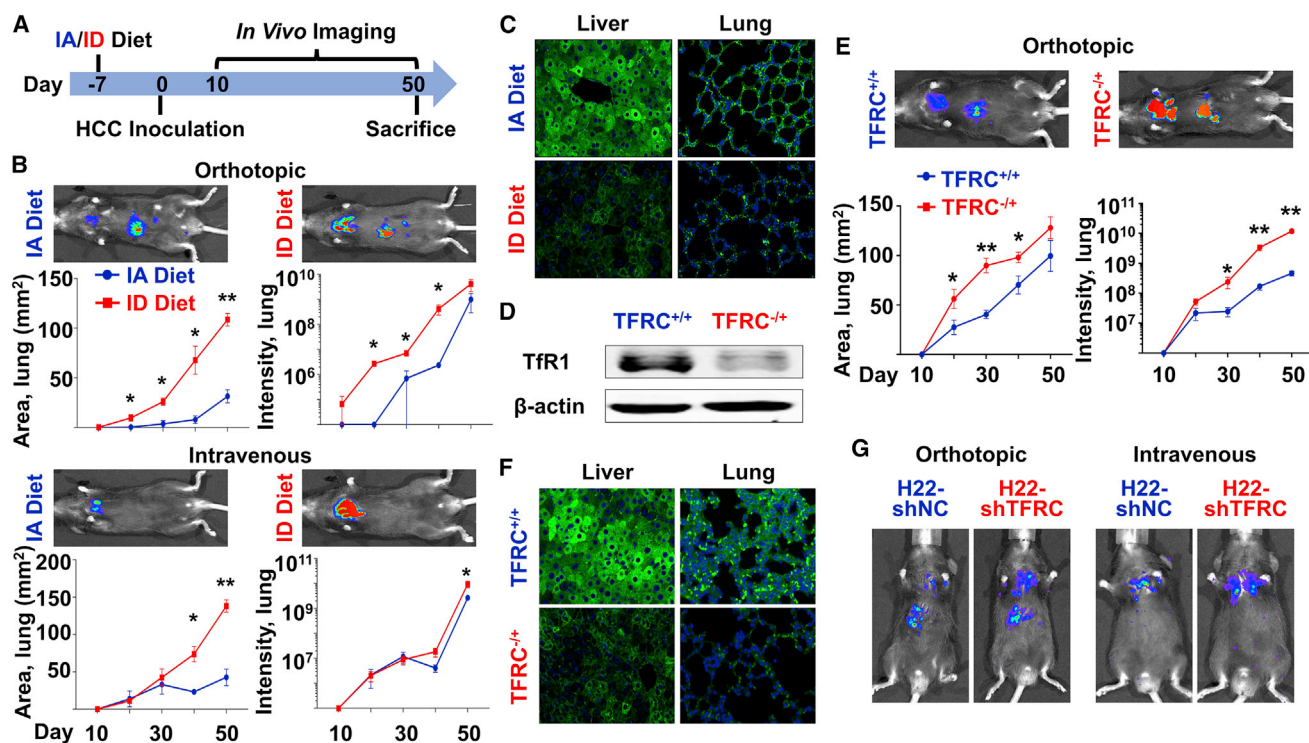
Figure 2. HCC pulmonary metastasis was increased under ID *in vivo*

(A–C) C57BL/6 mice were fed with either IA or ID diet at day −7. Mouse HCC H22 cells were orthotopically or intravenously administrated at day 0. All mice were sacrificed at day 50. n = 3 (A) Protocol for *in vivo* imaging. (B) Growth of tumor cells over time in the lung of mice. Representative figures were taken at day 50. (C) Ferritin expression in the liver and lung of the orthotopically injected mice. (D–F) WT (+/+) and TFRC heterozygous knockout (−/+) C57BL/6 mice were fed with IA diet at day −7. Mouse HCC H22 cells were orthotopically administrated at day 0. All mice were sacrificed at day 50. n = 6 (D) TFRC expression in the liver. (E) Growth of tumor cells over time in the lung of mice. Representative figures were taken at day 50. (F) Ferritin expression in the liver and lung. (G) C57BL/6 mice were fed with IA diet at day −7. TFRC-knockdown (shTFRC) mouse HCC H22 cells or their control counterparts (shNC) were orthotopically or intravenously administrated at day 0. Representative figures were taken at day 50. n = 3. The quantification data of Figure 2G are presented in Figure S3D. Data were presented as mean ± SEM. *p < 0.05, **p < 0.01 versus IA Diet or versus TFRC$^{+/+}$. IA, iron-adequate; ID, iron-deficient.

liver tissues with their own malignant tissues. It was evident that 39 out of 50 patients showed higher TFRC expression (Figure S1A) in the tumor tissues compared to NT tissues, while 47 out of 50 patients showed lower HAMP expression (Figure S1B) in the T samples. These data suggested that most HCC tumors were suffering ID status. The overall survival curves were plotted and compared between the low expression and high expression groups of each subpanels (Figure 1F). As a result, the high expression of TFRC, but not HAMP, predicted worse patient survival (p < 0.001).

ID enhanced HCC pulmonary metastasis

We first observed that in an orthotopic mouse model, the HCC tumor had less iron than N liver (Figure S2), consistent to the date of above clinical HCC samples. To study the roles of ID during HCC metastatic colonization *in vivo*, we fed 4- to 5-week-old C57BL/6 mice with either iron-adequate (IA) or ID diet, followed by orthotopic or intravenous administration of H22 mouse HCC cells (Figure 2A). In both cases, HCC pulmonary metastasis was significantly enhanced upon ID (Figure 2B). Tissues and serum were obtained at sacrifice. Iron indices (Table 1), as well as expression of ferritin light polypeptide

(FTL) in the liver and lung (Figure 2C), showed significant alteration upon ID diet.

In addition to the diet model, a genetically modified ID mouse model was generated to heterozygously knock out the TFRC protein 1 in whole body (TFRC$^{-/+}$), since homozygous knockout is lethal. Significantly reduced expression of TfR1 in the liver was detected by western blot analysis (Figure 2D). It was evident that orthotopically administrated H22 cells in the TFRC$^{-/+}$ mice showed greater metastasis than those cells injected in the N mice (Figure 2E). Liver and serum iron indices were obtained at sacrifice and indicated the statues of ID (Table 1), which was also confirmed by fluorescent immunostaining of FTL in both the liver and lung tissues (Figure 2F).

To exclude the effect of ID on N tissues, we manipulated the H22 cell line by lenti-vectors to permanently knock down the TFRC gene (shTFRC). Both mRNA (Figure S3A) and protein (Figure S3B) expression demonstrated that the knockdown efficiency was more than 70%. Phen Green-FL fluorescence signal quenching assay showed significantly decreased iron accumulation in the

Table 1. Liver, lung, and serum iron indices in various mouse models

	C57BL/6		TFRC-KO		Nude	
	IA diet	ID diet	WT	KO	IA diet	ID diet
Liver iron (μg/g)	74.05 ± 6.2	48.10 ± 1.9**	73.04 ± 10.0	43.62 ± 2.0*	76.59 ± 6.6	51.32 ± 3.4**
Lung iron (μg/g)	14.34 ± 3.3	4.21 ± 1.2*	N/A	N/A	26.91 ± 3.9	14.39 ± 3.0*
Serum iron (μmol/L)	27.62 ± 10.0	16.44 ± 2.8*	29.07 ± 1.6	19.56 ± 1.4**	51.12 ± 2.4	27.75 ± 3.1**
Serum TIBC (μmol/L)	54.98 ± 4.1	53.10 ± 7.6	65.96 ± 1.5	54.82 ± 1.1**	67.32 ± 2.7	57.74 ± 4.1
Serum TS (%)	51.03 ± 17.6	31.20 ± 5.8*	46.96 ± 3.4	34.83 ± 3.1*	71.33 ± 4.3	53.6 ± 3.0*
Serum ferritin (ng/mL)	2247 ± 998.5	1869 ± 319.6	2490 ± 217.7	1608 ± 90.3**	499.2 ± 77.4	520.7 ± 28.3

Note: All tissue and serum samples were obtained from HCC-bearing mice after perfusion at sacrifice. Data from orthotopically and intravenously injected mice were combined. n = 6, mean ± SD. *$p < 0.05$, **$p < 0.01$.

H22-shTFRC cells (Figure S3C). Then, those cells and their negative control counterparts were administrated into the C57BL/6 mice. The H22-shTFRC cells also exhibited significantly increased metastasis ability with a rout-independent manner (Figure 2G). The quantification data of Figure 2G are presented in Figure S3D. Little difference was observed in the expression of FTL in the N liver and lung, indicating the status of IA of host mice at sacrifice (Figure S3E). These data suggested that ID could increase *in vivo* HCC metastasis through both N and malignant liver cells, regardless of injection routs.

**SPNS2 expression was functionally increased under ID *in vivo***
Recently, S1P transporter spinster homolog 2 (SPNS2) was reported to be associated with pulmonary metastasis of various cancer cell types.[19] To evaluate the effect of ID on the SPNS2 expression *in vivo*, we separated N hepatocytes and HCC tumors from the liver of orthotopically administrated mice, which were fed with either IA or ID diet (Figure 2A). It was evident that ID altered the expression of iron-related genes *in vivo*, such as TFRC, HAMP, and FTL (Figure 3A). Meanwhile, in both N hepatocytes and tumor cells, ID led to significantly increased SPNS2 expression at the mRNA (Figure 3A) and protein levels (Figure 3B). SPNS2 is a significant and physiologically relevant transporter of S1P, a signaling sphingolipid that is present at high concentrations in blood. We performed liquid chromatography-mass spectrometry (LC-MS) assay to detect the S1P content in the serum of mice under ID. The results showed that ID increased serum S1P content (Figure S4), consistent with previous reports that overexpression of SPNS2 in mammalian cells increased the secretion of S1P.[21] Since SPNS2 is a key regulator for immune cell survival,[22] we characterized the phenotype of lymphatic subsets in the liver and lung of tumor-bearing mice. Flow cytometry assays revealed that ID led to a profound reduction in the percentage of B, T, and natural killer (NK) cells (Figure 3C), which is corroborated by immunofluorescence staining against CD8$^+$ and CD69$^+$ cells (Figure S5). Further, the ID mice liver contained a significantly lower percentage

of effector T cells, with a similar phenotype seen in the lung (Figure 3C). In another ID mouse model, genetically modified TFRC$^{-/+}$ mice, flow cytometry assays also revealed lower percentage of B, T, and NK cells, as well as that of effector T cells, compared to the wild-type (WT) mice (Figure 3D). In addition to the mouse samples, we also analyzed the tumor tissues from patients with or without metastasis. It was evident that tumors with metastasis tended to express higher levels of TFRC and SPNS2 than their counterparts without metastasis (Figures 3E and 3F). To quantify SPNS2-associated cell-infiltrating patterns in tumor microenvironment, we obtained gene-expression profiles of HCC tissues from the TCGA database and divided patients into two groups based on the lower and upper quartile of transcripts per million values of SPNS2. The data were uploaded to the Cell-Type Identification by Estimating Relative Subsets of RNA Transcripts (CIBERSORT) web portal (http://cibersort.stanford.edu/) and were analyzed by the algorithm using the LM22 signature and 1,000 permutations.[23] As demonstrated in the Figure S6, the HCC tissues with low SPNS2 expression showed less infiltration of CD8-positive T cells, T follicular helper cells, and activated NK cells compared to the HCC tissues with high SPNS2 expression. Taken together, our data suggested the role of SPNS2 in tumor microenvironmental regulation during ID-induced HCC metastasis.

SPNS2 is involved in ID-induced HCC pulmonary metastasis in an immune-independent manner
Given that TFRC-knockout H22 cells led to enhanced pulmonary metastasis in mice fed with IA diet (Figure 2G), we hypothesized that ID may induce HCC metastasis in an immune-independent manner *in vivo*. To this end, nude mice with an inhibited immune system were fed with either IA or ID diet, followed by orthotopic or intravenous administration of human Huh7 liver cancer cells. The protocols were the same as shown in Figure 2A. Consistent with the above observations, human HCC pulmonary metastasis was significantly enhanced upon ID diet, regardless of HCC injection routs (Figure 4A). Liver and serum iron indices were obtained at sacrifice (Table 1) and indicated the statues of ID, which was also confirmed by the immunostaining of ferritin in the liver and lung (Figure S7). N hepatocytes and HCC tumors were separated from the liver of orthotopically administrated mice, both of which were subjected to qRT-PCR and western blot assays to determine the expression of iron-related genes and SPNS2 (Figure 4B). ID diet led to not only alternated expression of the iron-related genes, but also significantly enhanced SPSN2 expression at both the mRNA and protein levels.

To restrict the effect of ID on the tumor cells, we knocked down the TFRC expression (TFRC-KD) in human Huh7 cells. Quantitative real-time PCR (Figure S8A), western blot (Figure S8B), and Phen Green-FL fluorescence signal quenching assays (Figure S8C) indicated the reduced TFRC mRNA, TfR1 protein, and iron accumulation, respectively. Most importantly, the TFRC-KD cells showed significantly increased metastasis in the nude mice (Figure S8D), independent of the tumor cell administration routes.
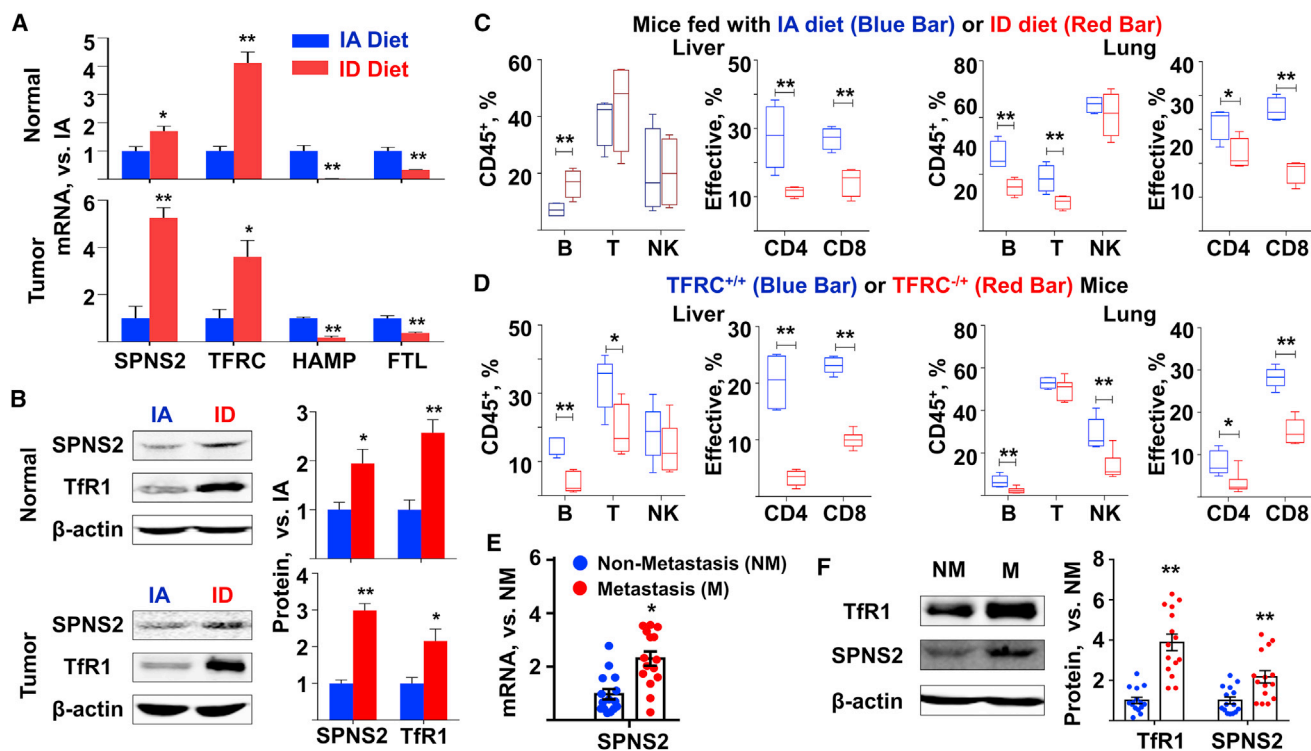
**Figure 3. ID was associated with increased SPNS2 expression**

(A and B) N and T tissues in the liver were sectioned from the orthotopically administrated mice in Figure 2B. n = 3. (A) mRNA and (B) protein expression of SPNS2 and iron-related genes were determined. (C and D) Liver and lung tissues were sectioned from the orthotopically administrated (C) C57BL/6 mice in Figure 2B or (D) the WT (TFRC^{+/+}) and TFRC-knockout (TFRC^{−/+}) mice in in Figure 2E. The percentage of lymphocyte subsets and that of effective T cells in the liver (left) and lung (right) were determined by flow cytometry assay. Effective: CD 44^{high}, CD62^{low}. n = 3. (E) The mRNA and (F) protein expression of TFRC and SPNS2 in the human M and NM HCC tumors in Figure 1D. N = 15. Data were presented as mean ± SEM. *$p < 0.05$, **$p < 0.01$ versus IA diet, versus N mice, or versus NM. SPNS2, transporter spinster homolog 2.

Furthermore, a recently developed NOD.Cg (NCG) mouse model, which lacks proper T cell, B cell, and NK cell production, was used to test our hypothesis. The results demonstrated that the NCG mice with ID diet phenocopied the pulmonary metastasis of the nude mice, further validating the importance of an immune-independent role of SNPS2 in control of pulmonary metastatic burden (Figure 4C). It is worthy noticing that the tumor-cell-specific TFRC knockdown, which resulted in ID only in the tumor cells, also led to significant increased HCC metastasis in the NCG mice (Figure 4D).

The role of ID and SPNS2 in HCC cell lines *in vitro*

We would like to further investigate the mechanism of ID-enhanced HCC metastasis in cell cultures *in vitro*. The IC$_{50}$s of two iron chelators, Dp44mT and DFO, were determined as 4.986 μM and 60.579 μM, respectively, in the Huh7 cells (Figure S9). Thus, 2 μM Dp44mT and 10 μM DFO were used to treat various HCC cell lines, which led to cell growth inhibition (Figure 5A; Figure S10), consistent with previous reports.[24] Meanwhile, we observed significant increases in the migration and invasion abilities of those cell lines *in vitro* (Figure 5B; Figures S11A and S11B). In agreement with previous reports, upon ID treatment, the expression of TFRC was significantly increased, while that of FTL was reduced (Fig-

ure 5C; Figures S12 and S13). Interestingly, the SPNS2 expression in all the above HCC cell lines was increased upon ID treatment. As appropriate controls, human and mouse primary hepatocytes were cultured *in vitro* and treated with iron chelators. At both mRNA and protein levels, ID led to elevated SPNS2 expression and altered expression of iron-related genes in primary hepatocytes (Figure 5D), which was consistent with the above *in vivo* studies. It is worth noticing that upon ID treatment, HAMP levels of hepatic cell cultures (Figures 5C and 5D; Figure S12) did not respond as they did *in vivo* (Figures 3A and 4B). In some cases, HAMP expression was even increased with iron chelator treatment (Figure S12C). Next, we designed three SPNS2-targeting small interfering RNA (siRNA) sequences and their negative control (siNC), one of which showed more than 50% inhibitory efficiency in various HCC cell lines (Figure S14A). Western blot assay further confirmed that the SPNS2 expression was significantly reduced upon siRNA treatment (Figure 5E; Figures S14B and S14C). Co-treatment of human HCC cell lines with siRNA against SPNS2 and iron chelator rescued the ID-enhanced migration and invasion abilities of the HCC cell lines (Figure 5F; Figures S14D and S14E). To explore the potential mechanisms for SPNS2-induced metastasis, we analyzed an iron-responsive gene-expression profile in the mice liver that was fed with either
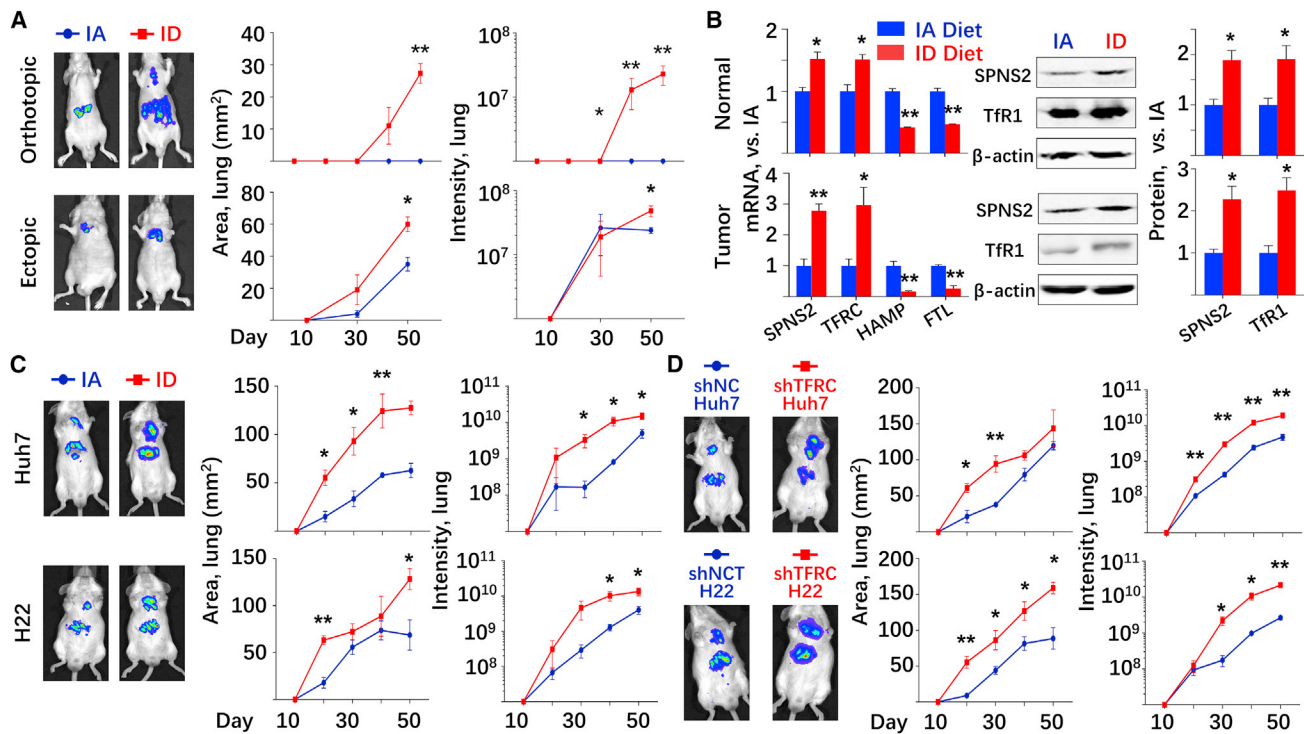
Figure 4. SPNS2 affected ID-enhanced HCC metastasis in an immune-independent manner *in vivo*
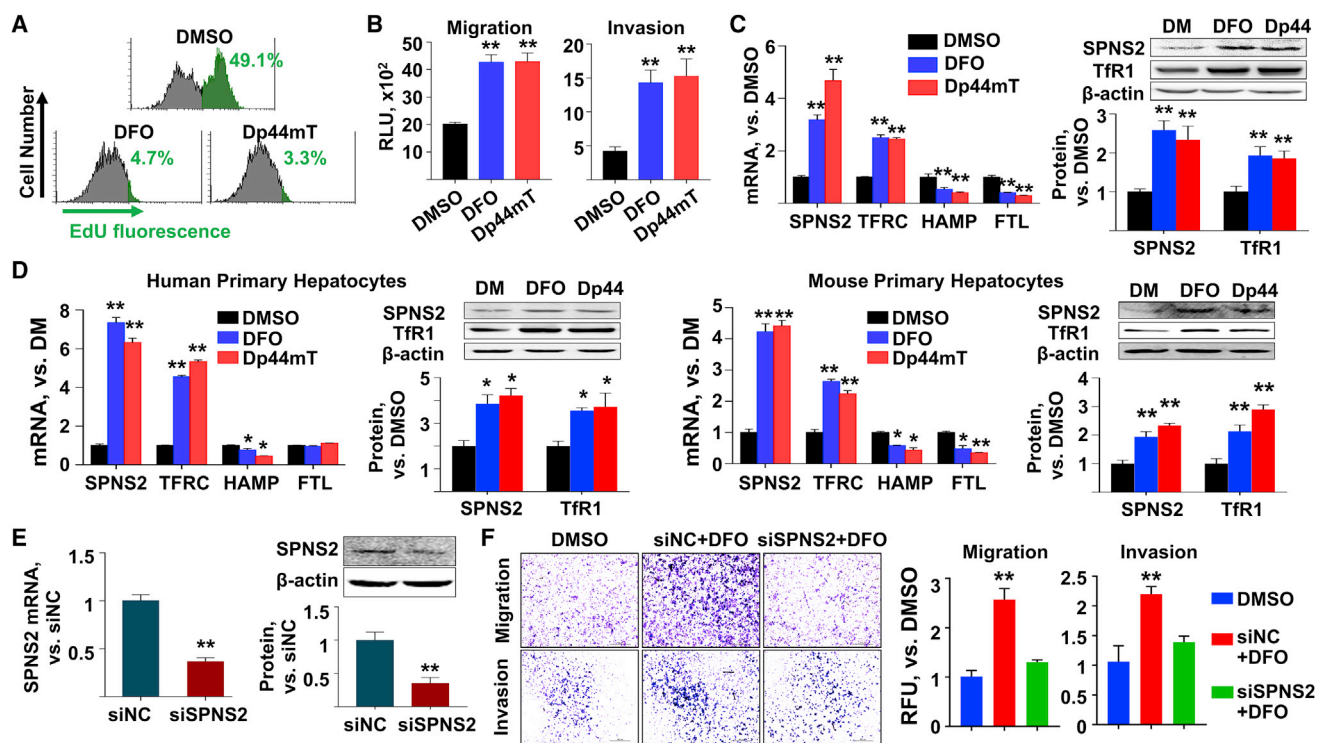
(A and B) Nude mice were fed with either IA or ID diet at day −7. Human HCC Huh7 cells were orthotopically or intravenously administered at day 0. All mice were sacrificed at day 50. Representative figures were taken at day 50. n = 3. (A) Growth of tumor cells over time in the lung of mice. (B) N and T tissues in the liver were sectioned from the orthotopically administered mice. mRNA and protein expression of SPNS2 and iron-related genes were determined. (C and D) Growth of tumor cells over time in the lung of mice. (C) NCG mice were fed with either IA or ID diet at day −7. Human HCC Huh7 cells (upper) or mouse HCC H22 cells (lower) were orthotopically administered at day 0. (D) NCG mice were fed with IA diet at day −7. TFRC-knockdown Huh7 cells (upper) or H22 cells (lower) and their control counterparts were orthotopically administered at day 0. Representative figures were taken at day 50. Data were presented as mean ± SEM. *p < 0.05, **p < 0.01 versus IA diet, or versus shNC.

ID, IA, or IO diet. The Gene Ontology (GO) and Kyoto Encyclopedia of Genes and Genomes (KEGG) enrichment analysis showed that the genes involved in migration, angiogenesis, kinase phosphorylation, growth factor activity, and focal adhesion (Figure S15A) and genes involved in PI3K-Akt, Ras, and mitogen-activated protein kinase (MAPK) signaling pathway (Figure S15B), respectively, were significantly affected by diet iron. We then validated the top 10 altered genes in the human liver cancer samples (Figure S16A) and iron chelator treated Huh7 cells (Figure S16B). Interestingly, expressions of TEK, ENPEP, SIRPA, and BMP2 were consistently affected. Although further studies are warranted, our results indicated that ID enhanced HCC metastasis *in vitro* through the SPNS2 signaling pathway.

Inhibition of SPNS2 expression *in vivo* abolished ID-promoted HCC pulmonary metastasis

We first generated germline SPNS2-knockout C57BL/6 mice using CRISPR-Cas9. Genome typing assay confirmed the loss of intact SPNS2 gene (Figure 6A; Figure S17). This resulted in an overall decreased metastatic burden after orthotopic administration with HCC cells (Figure 6B). While ID induced HCC metastasis in the WT mice, it has no effect in the tumor-bearing SPNS2-knockout mice (Fig-

ure 6B). Liver and lung tissues were obtained at sacrifice. In agreement with previous studies,[19] globally deletion of SPNS2 created a lower T and B cells, as well as higher percentage of effector CD4^{+} and CD8^{+} T cells present in both the liver and lung (Figure 6C). To further corroborate our observation, we packaged the short hairpin RNA (shRNA) against SPSN2 into a recombinant AAV (rAAV) serotype 8 vector (Figure S18A), which is well known to efficiently target mice hepatocytes.[25] The experimental protocol is schematically presented as Figure S18B. Indeed, the bio-distribution assay at 4 weeks post-viral injection indicated that the majority of viral vector genomes (Figure S18C) and transgene expression (Figure S18D) were limited in the liver after tail-vein administration. The functional loss of SPNS2 in the liver was indicated by both western blot assay (Figure 6D) and flow cytometry assay detecting various immune cell types (Figure S18E). The viral vector injected mice were fed with either IA or ID diet, followed by orthotopic administration with HCC cells. Consistent to our above studies, ID enhanced HCC pulmonary metastasis in the mice that were injected with control rAAV vectors (Figure 4E). However, in those injected with rAAV-shSPNS2 vectors, ID had no significant effect (Figure 4E). Taken together, our data demonstrated that loss of SPNS2, either globally or in a hepatocyte-specific manner, abolished ID-induced HCC pulmonary metastasis *in vivo*.

Figure 5. ID enhanced HCC cell migration and invasion *in vitro*

(A–D) Huh7 cells or primary hepatocytes were treated with either dimethyl sulfoxide (DMSO) or iron chelators, deferoxamine (DFO) and Dp44mT, for 24 h. (A) The number of dividing Huh7 cells were determined by EdU fluorescence levels. (B) Migration and invasion ability of Huh7 cells under ID. (C and D) The mRNA (left) and protein (right) expression of SPNS2 and iron-related genes in the (C) Huh7 cells and (D) primary human and mouse hepatocytes under ID. See experiment results using other HCC cell lines in Figures S8–S10. (E) Efficiency of siRNA-mediated SPNS2 knockdown in the Huh7 cells. (F) Huh7 cells were transfected with siRNA against SPSN2 and co-treated with either DMSO or DFO for 24 h. Migration and invasion abilities of SPNS2 knockdown Huh7 cells under ID. Representative figures were shown. See experiment results using other HCC cell lines in Figure S12. All *in vitro* experiments were performed as 3 replications. Both representative figures and quantitative data of western blot assays were shown. Data were presented as mean ± SEM. *p < 0.05, **p < 0.01 versus DMSO, or versus siNC. Edu, 5-ethynyl-2′-deoxyuridine.

DISCUSSION

Increased expression of TFRC and decreased HAMP have been found in HCC in animal studies,[26] and more recently, in clinical samples.[27,28] It was believed that more aggressive tumors grow more rapidly and, therefore, have higher iron requirements, resulting in higher TFRC expression. The results presented here expand the above understanding, showing that the growing HCC tumors are at the statues of ID. Most importantly, our data provide a mechanistic link, SPNS2, between the ID phenotype and HCC metastasis. Previous studies focused on the functions of SPNS2 in immune system, which may account for its recently discovered unexpected importance in cancer metastasis.[19] There was little effort to elucidate a role for SPNS2 in cancer cells themselves. It is worth noticing that in their pioneering work, Kawahara et al.[21] documented that SPNS2 regulates myocardial precursor migration. However, how SPNS2 regulates cancer cell migration is unknown. The only report suggested the association of SPNS2 with increased EGF-mediated invasion of HeLa cells *in vitro*.[29] Our studies not only demonstrated a direct role of SPNS2 in HCC metastasis, but also suggested the importance of its potential upstream regulator, iron.

Under ID, the reduction of HAMP is a host adaptation mechanism that facilitates iron absorption *in vivo*, while *in vitro* studies have provided conflicting results. Several independent groups recently documented that DFO treatment slightly upregulated HAMP mRNA in cultured cells.[30,31] Although the exact underlying mechanism requires further studies, iron chelation appeared to slightly impair signaling to HAMP in the DFO-treated cells.[32] Thus, in our studies, we also detected TFRC and Ferritin expression to confirm the conditions of ID *in vitro*. The understanding of the contribution of iron in carcinogenesis and tumor progression has advanced considerably in recent years. However, a role for iron in cancer metastasis is largely unexplored. High ferroportin and low HAMP gene expression was suggested as a favorable cohort of breast cancer patients who have a 10-year survival of >90%,[33] suggesting that the effect of iron on metastasis is cancer-type-dependent. Nevertheless, the underlying mechanism how iron disruption regulates SPNS2 expression is currently under evaluation in our laboratory. In addition, altered expression of proteins of iron metabolism may affect tumor cells in an iron-independent manner, such as epithelial mesenchymal transition.[34] It is of interest to evaluate the effect of ID on these biological processes. HCC has a high risk of
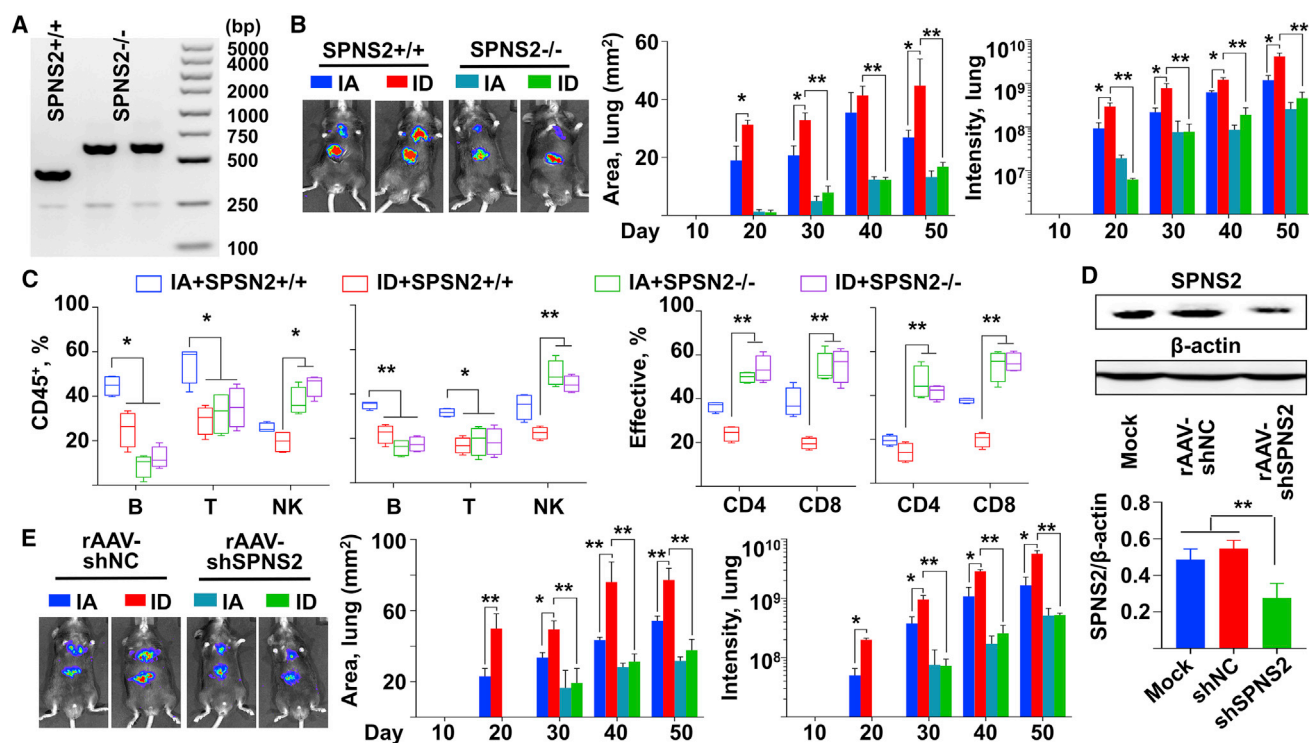
Figure 6. Inhibition of SPNS2 reduced the effect of ID on HCC pulmonary metastasis *in vivo*

(A) Genome typing of the WT (SPNS2^{+/+}, 409bp) and SPNS2-knockout (SPNS2^{−/−}, 613 bp) mice. (B and C) WT and SPNS2-KO mice were fed with either IA or ID diet at day −7. Mouse HCC H22 cells were orthotopically administrated at day 0. All mice were sacrificed at day 50. n = 4. (B) Growth of tumor cells over time in the lung of WT and SPNS2-KO mice. Representative figures were taken at day 50. (C) The percentage of lymphocyte subsets and that of effective T cells in the liver (left) and lung (right) were determined by flow cytometry assay. Effective: CD 44^{high}, CD62[Low]. (D) The SPNS2 expression in the liver of C57BL/6 mice at 1 month-post rAAV vector administration. Both representative figures and quantitative data of western blot assay were shown. n = 3. (E) Growth of orthotopically injected mouse HCC H22 cells over time in the lung of C57BL/6 mice, following rAAV8 vector administration. See protocols for *in vivo* imaging in Figure S5A. Representative figures were taken at day 50. n = 3. Data were presented as mean ± SEM. *p < 0.05, **p < 0.01.

multi-centric (MC) tumor occurrence and intrahepatic metastasis (IM) due to a strong carcinogenic background in the liver.[35] MC and IM tumors are profoundly different in terms of their development, growth, metastasis, and clinical outcome. In addition, other routes of HCC spread had been recently revealed due to novel imaging techniques. For example, although rare, bone metastases in HCC are ultra-aggressive and optimal treatment strategies are warranted.[36] Further study is needed to elucidate whether iron and SPNS2 are involved in these types of metastasis.

Taken together, we demonstrated here that ID increased pulmonary metastasis of HCC. Mechanistically, iron depletion increased SPNS2 expression in both N hepatocytes and HCC cancer cells. This increase may create a lower percentage of effector T cells and natural killer cells, allowing for an overall enhanced metastatic burden. Meanwhile, SPSN2 overexpression in the HCC cells promotes their migration and invasion abilities. While iron chelator DFO was used in clinical trials to treat various solid cancers[37,38] and was proposed for advanced HCC,[14] the data presented here, on the other hand, suggested that iron chelation therapy shall be cautiously used to treat HCC patients. Most importantly, AAV vectors are the leading platform for gene de-

livery for the treatment of a variety of human diseases, with the recent FDA approval of two AAV drugs for inherited blindness and spinal muscular atrophy.[23] Considering the extreme complexity and tight regulation of iron metabolism, instead of directly targeting iron for treatment, our mechanistic studies suggest SPNS2 as a potential therapeutic target for the prevention of HCC pulmonary metastasis.

MATERIALS AND METHODS

Cells and chemicals

Huh7 and HepG2 cells were cultured in high glucose DMEM (GIBCO, CA, USA); SMMC-7721 cells and H22 cells were cultured in RPMI-1640, both containing 10% fetal bovine serum (GIBCO, CA, USA). Human and mouse primary hepatocytes were cultured in hepatocyte medium with addition of 10% fetal bovine serum and hepatocyte growth supplement (ScienCell, CA, USA). All primary cells were purchased from ScienCell (CA, USA) with STR Authentication. Iron chelators DFO (Cat#. S6849) and Dp44mT (Cat#. S7909) were purchased from Selleck Chemicals (TX, USA). Lipofectamine 3000 (Thermo Fisher, USA) was used to transfect siRNA or plasmid for cells as previously described.[39] The Phen Green FL reagent for

fluorescence quenching assay was purchased from Thermo Fisher, USA

Western blot

Total proteins of tissues or cells were extracted with the protein extraction kit (Keygene Biotech, Nanjing, China). Antibodies used in this study were: SPNS2 (1:500, Abcam, USA), TfR1 (1:1,000, Abcam, USA), HAMP (1:500, Abcam, USA) and β-actin (1:2,000, Sangon Biotech, China). The IRDye secondary antibody (1:10,000, LI-COR, USA) was used and immunoblots was scanned by Odyssey dual-color infrared fluorescence imaging system. Grayscale of each band was obtained from Odyssey software.

Quantitative real-time PCR analysis

Total RNAs were extracted by Trizol (Thermo Fisher, USA), purified by RNeasy mini kit (QIAGEN, USA) and reverse-transcribed by PrimeScript RT Master Mix (Takara, Japan). Quantitative real-time PCR were performed by the SYBR Green Kit (Toyobo Bio, Japan) using StepOnePlus system (Applied Biosystems, USA). All primers are listed in Table S1. The results were normalized to 18 s.

Fluorescence quenching assay

For detection of the intracellular iron, we applied fluorescence quenching method with the Phen Green FL reagent (Thermo Fisher, USA), following the manufacturer's instructions.

Cell proliferation, migration, and invasion

The Click-iT Plus 5-ethynyl-2′-deoxyuridine (EdU) Alexa Fluor 488 Flow Cytometry Assay Kit (Thermo Fisher, USA) was used to determine proliferation of cells. CytoSelect 96-Well Cell Migration Assay Kit and Invasion Assay kit (Cell Biolabs, USA) were used to determine the migration and invasion abilities of HCC cells, respectively.

Animals

Animal experiments were approved by the Ethics Committee of the Second Military Medical University and all operations followed the norms of humane care. All mice were operated in specific-pathogen-free (SPF) or sterile environment in Animal Center of the Second Military Medical university, with N circadian rhythm and food or water *ad libitum*. 4- to 5-week old C57/BL6 mice and nude mice were purchased from Animal Center of the Second Military Medical University. NCG mice were purchased from Model Animal Research Center of Nanjing University (Cat. T001475, NOD-Prkdc[em26] Il2rg[em26]). TFRC knockout mice were purchased from Model Animal Research Center of Nanjing University (Cat. T002444, B6/J-TFRC[em1Cd/Nju], heterozygote) with deletion of 202 bp in exon3 by Cas9 system. The WT product (1,776 bp) and knockout product (971 bp) were detected by primers TFRC-sg-5in-tF and TFRC-sg-3in-tR, listed in Table S2. Construction of SPNS2 knockout C57/BL6 mice were commissioned to Cyagen Biosciences Inc. The exon3-5 of SPNS2 gene were deleted by Cas9 system. The guide RNAs were listed in Table S3. The WT product (409 bp) and knockout product (613 bp) were detected by primers SPNS2-F1/SPNS2-R1 and SPNS2-F2/SPNS2-R1, listed in the Table S2. At the

end of the experiments, serum was collected through facial bleeding. All mice were sacrificed, followed by immediate perfusion to minimize blood contamination.

Animal diet and HCC inoculation

Animal diet was purchased from Trophic Animal Feed High-Tech (Nantong, China). The iron adequate diet (Cat#. TP0304C) and ID diet (Cat#. TP0304) contained 45 ppm iron and 3 ppm iron, respectively. Mice were 4–6 weeks old when the ID diets were started. The mice were on diet for 1 week prior to administration of HCC cells. HCC cells were mixed with matrigel (2×10^7/mL) and 0.1 mL cells suspension was orthotopically injected into the liver. The intravenous injection of HCC cells was carried out with a slow injection (30 s∼40 s) of 0.1 mL cells suspension (1×10^7/mL) through the tail vein.

In vivo imaging

Mice were photographed every 10 days after injection of HCC cells. The tumor-bearing mice were anesthetized by isoflurane inhalation and intraperitoneally injected with D-Luciferin (150 μL, 10 mg/mL). The photograph was taken and analyzed by *in vivo* imaging system (IVIS Lumina LT Series III, PerkinElmer, USA). Luciferase Substrates D-Luciferin was purchased from Sigma-Aldrich (USA).

Iron status parameters

Liver iron level was quantitated using an atomic absorption spectrophotometer (Z-8100, Hitachi, Tokyo, Japan) and normalized to the wet tissue weight for each sample. Serum iron concentrations, transferrin binding capacity (TIBC) and transferrin saturation (TS%) in non-hemolyzed serum samples were determined by Hitachi 7600 Automatic Biochemical Analyzer. Serum ferritin content was detected by ELISA kit (Immunology Consultants Laboratory, USA) following its instructions. The iron status of the mice was determined upon sacrifice of mice.

Immunofluorescence analysis

Liver tissues or lung tissues were fixed in 4% paraformaldehyde. Slices of tissues were cut by a semiautomatic freezing microtome and incubated with ferritin (Abcam, USA), CD8 (Abcam, USA), or CD69 (Abcam, USA). The nucleus was stained by DAPI. After incubation with secondary antibody of Alexa Fluor 488 (Abcam, USA), the slices were pictured by an inverted fluorescent microscope (Leica, Germany).

Recombinant AAV vector production

Preparation and purification of recombinant AAV vectors by triple-plasmid transfection have been described previously.[25] All vector preparations were subjected to quality control tests including western blot analysis, qPCR, and Southern blot analysis. The highly purified rAAV vectors were then intravenously via tail vein into IO mice at 10E11 viral genome/mouse.

Determination of iron content by MRI

GE Signa HDX 1.5T MR scanner was used to scan the HCC patients before surgical operation according to the set parameters as before.[40] T2* weighted scan was conducted and R2* map was created

accordingly by workstation software to obtain the R2* value, which could represent iron content, of manually marked area of interest (AOI) in R2* map.

Detection of lymphocyte subsets proportion

Total white cells of the liver or the lung were extracted by using white cell extraction kit (Cat#. WBC1092Z, TBDscience, Tianjin, China) according to its instructions. Then the white cells were incubated with different antibodies to lymphocyte surface antigens for 30 min at 37°C. All antibodies were purchased from eBioscience (Thermo Fisher, USA): CD45 (Cat#. 12-0451-81), CD19 (Cat#, 11-0193-81), CD3 (Cat#, 17-0032-80), NK1.1 (Cat#, 45-5941-80), CD4 (Cat#, 17-0041-81), CD8 (Cat#, 45-0081-80), CD44 (Cat#, 12-0441-81), and CD62L (Cat#, 11-0621-82). By detecting fluorescence signals of cells using flow cytometry (Beckman Coulter, USA), the proportions of lymphocyte subsets in white cells were obtained. Cells with CD45 positive signal were regarded as white cells, from which $CD3^+$, $CD19^+$, and $NK1.1^+$ were used to represent the proportion of T, B, and NK cells, respectively. $CD4^+CD44^{hi}CD62L^{lo}/CD4^+$ and $CD8^+$ $CD44^{hi}CD62L^{lo}/CD8^+$ were used to represent the proportion of effector $CD4^+$ and $CD8^+$ T cells, respectively.

Patients

The enrollment of patients was described before.[41] Written informed consent was received from participants prior to inclusion in the study. T samples and their NT counterparts were used. Each patient received a histopathological diagnosis based on the World Health Organization criteria. The histological tumor differentiation was determined according to the system proposed by Edmondson and Steiner. The Research Ethics Committees of Zhongshan Hospital, Fudan University, Shanghai, China, and of Changhai Hospital, Second Military Medical University granted ethical approval for the use of human subjects. We diagnosed tumor metastasis based on computed tomography scans, magnetic resonance imaging, digital subtraction angiography, and elevated serum alpha-fetoprotein (AFP) level, with or without histological confirmation. The surviving patients were censored at the time of the end of follow-up.

Statistics

t test was used for two-group comparison and one-way ANOVA followed by Bonferroni's test was used for multi-group comparison, if the data obey the normal distribution. In the case that the data do not obey the normal distribution, Mann-Whitney test was used for two-group comparison and Kruskal-Wallis test was used for multi-group comparison. A p value < 0.05 was considered as significantly different: $p < 0.05$ (*), $p < 0.01$ (**).

Ethical approval and consent to participate

Each patient received a histopathological diagnosis based on the World Health Organization criteria. Research involving human material has been performed in accordance with the Declaration of Helsinki. The Research Ethics Committees of Zhongshan Hospital, Fudan University, Shanghai, China, and of Changhai Hospital, Second Military Medical University granted ethical approval for the use of human subjects.

Availability of data and materials

All data generated or analyzed during this study are included in this published article and its supplemental information files. The datasets are available from the corresponding author on reasonable request.

SUPPLEMENTAL INFORMATION

Supplemental information can be found online at https://doi.org/10.1016/j.ymthe.2021.09.012.

AUTHOR CONTRIBUTIONS

M.L., Y.T., and D.W. performed *in vitro* experiments. Y.T., and X.Z. performed animal intervention. H.S., and M.Y. assessed, measured, and quantified the results of *in vivo* experiments. A.J., and M.Y. performed MRI experiments. C.Z. and C.L. analyzed the rAAV vectors and performed related *in vivo* experiments. S.Z., Z.Z., and J.F. were responsible for human-related data. M.L. and C.L. designed experiments. J.F., C.-q.L., and C.L. analyzed the data and wrote the manuscript.

DECLARATION OF INTERESTS

The authors declare no competing interests.

REFERENCES

1. Bray, F., Ferlay, J., Soerjomataram, I., Siegel, R.L., Torre, L.A., and Jemal, A. (2018). Global cancer statistics 2018: GLOBOCAN estimates of incidence and mortality worldwide for 36 cancers in 185 countries. CA Cancer J. Clin. *68*, 394–424.

2. Rankin, E.B., and Giaccia, A.J. (2016). Hypoxic control of metastasis. Science *352*, 175–180.

3. Roberts, L.R., Sirlin, C.B., Zaiem, F., Almasri, J., Prokop, L.J., Heimbach, J.K., Murad, M.H., and Mohammed, K. (2018). Imaging for the diagnosis of hepatocellular carcinoma: A systematic review and meta-analysis. Hepatology *67*, 401–421.

4. Llovet, J.M., Ricci, S., Mazzaferro, V., Hilgard, P., Gane, E., Blanc, J.F., de Oliveira, A.C., Santoro, A., Raoul, J.L., Forner, A., et al.; SHARP Investigators Study Group (2008). Sorafenib in advanced hepatocellular carcinoma. N. Engl. J. Med. *359*, 378–390.

5. Sapisochin, G., and Bruix, J. (2017). Liver transplantation for hepatocellular carcinoma: outcomes and novel surgical approaches. Nat. Rev. Gastroenterol. Hepatol. *14*, 203–217.

6. Greten, T.F., Mauda-Havakuk, M., Heinrich, B., Korangy, F., and Wood, B.J. (2019). Combined locoregional-immunotherapy for liver cancer. J. Hepatol. *70*, 999–1007.

7. Ling, C.Q., Fan, J., Lin, H.S., Shen, F., Xu, Z.Y., Lin, L.Z., Qin, S.K., Zhou, W.P., Zhai, X.F., Li, B., and Zhou, Q.H.; Chinese Integrative Therapy of Primary Liver Cancer

Working Group (2018). Clinical practice guidelines for the treatment of primary liver cancer with integrative traditional Chinese and Western medicine. J. Integr. Med. 16, 236–248.

8. Torti, S.V., and Torti, F.M. (2013). Iron and cancer: more ore to be mined. Nat. Rev. Cancer 13, 342–355.

9. Torti, S.V., Manz, D.H., Paul, B.T., Blanchette-Farra, N., and Torti, F.M. (2018). Iron and Cancer. Annu. Rev. Nutr. 38, 97–125.

10. Pfeifhofer-Obermair, C., Tymoszuk, P., Petzer, V., Weiss, G., and Nairz, M. (2018). Iron in the Tumor Microenvironment-Connecting the Dots. Front. Oncol. 8, 549.

11. Gangaidzo, I.T., and Gordeuk, V.R. (1995). Hepatocellular carcinoma and African iron overload. Gut 37, 727–730.

12. Elmberg, M., Hultcrantz, R., Ekbom, A., Brandt, L., Olsson, S., Olsson, R., Lindgren, S., Lööf, L., Stål, P., Wallerstedt, S., et al. (2003). Cancer risk in patients with hereditary hemochromatosis and in their first-degree relatives. Gastroenterology 125, 1733–1741.

13. Musallam, K.M., Cappellini, M.D., Wood, J.C., and Taher, A.T. (2012). Iron overload in non-transfusion-dependent thalassemia: a clinical perspective. Blood Rev. 26, S16–S19.

14. Yamasaki, T., Terai, S., and Sakaida, I. (2011). Deferoxamine for advanced hepatocellular carcinoma. N. Engl. J. Med. 365, 576–578.

15. Louandre, C., Ezzoukhry, Z., Godin, C., Barbare, J.C., Mazière, J.C., Chauffert, B., and Galmiche, A. (2013). Iron-dependent cell death of hepatocellular carcinoma cells exposed to sorafenib. Int. J. Cancer 133, 1732–1742.

16. Li, M., Tang, Y., Wu, L., Mo, F., Wang, X., Li, H., Qi, R., Zhang, H., Srivastava, A., and Ling, C. (2017). The hepatocyte-specific HNF4α/miR-122 pathway contributes to iron overload-mediated hepatic inflammation. Blood 130, 1041–1051.

17. Tsai, W.C., Hsu, S.D., Hsu, C.S., Lai, T.C., Chen, S.J., Shen, R., Huang, Y., Chen, H.C., Lee, C.H., Tsai, T.F., et al. (2012). MicroRNA-122 plays a critical role in liver homeostasis and hepatocarcinogenesis. J. Clin. Invest. 122, 2884–2897.

18. Hsu, S.H., Wang, B., Kota, J., Yu, J., Costinean, S., Kutay, H., Yu, L., Bai, S., La Perle, K., Chivukula, R.R., et al. (2012). Essential metabolic, anti-inflammatory, and anti-tumorigenic functions of miR-122 in liver. J. Clin. Invest. 122, 2871–2883.

19. van der Weyden, L., Arends, M.J., Campbell, A.D., Bald, T., Wardle-Jones, H., Griggs, N., Velasco-Herrera, M.D., Tüting, T., Sansom, O.J., Karp, N.A., et al.; Sanger Mouse Genetics Project (2017). Genome-wide in vivo screen identifies novel host regulators of metastatic colonization. Nature 541, 233–236.

20. Andrieu, G., Ledoux, A., Branka, S., Bocquet, M., Gilhodes, J., Walzer, T., Kasahara, K., Inagaki, M., Sabbadini, R.A., Cuvillier, O., and Hatzoglou, A. (2017). Sphingosine 1-phosphate signaling through its receptor S1P₅ promotes chromosome segregation and mitotic progression. Sci. Signal. 10, eaah4007.

21. Kawahara, A., Nishi, T., Hisano, Y., Fukui, H., Yamaguchi, A., and Mochizuki, N. (2009). The sphingolipid transporter spns2 functions in migration of zebrafish myocardial precursors. Science 323, 524–527.

22. Spiegel, S., Maczis, M.A., Maceyka, M., and Milstien, S. (2019). New insights into functions of the sphingosine-1-phosphate transporter SPNS2. J. Lipid Res. 60, 484–489.

23. Newman, A.M., Liu, C.L., Green, M.R., Gentles, A.J., Feng, W., Xu, Y., Hoang, C.D., Diehn, M., and Alizadeh, A.A. (2015). Robust enumeration of cell subsets from tissue expression profiles. Nat. Methods 12, 453–457.

24. Ba, Q., Hao, M., Huang, H., Hou, J., Ge, S., Zhang, Z., Yin, J., Chu, R., Jiang, H., Wang, F., et al. (2011). Iron deprivation suppresses hepatocellular carcinoma growth in experimental studies. Clin. Cancer Res. 17, 7625–7633.

25. Ling, C., Wang, Y., Feng, Y.L., Zhang, Y.N., Li, J., Hu, X.R., Wang, L.N., Zhong, M.F., Zhai, X.F., Zolotukhin, I., et al. (2015). Prevalence of neutralizing antibodies against liver-tropic adeno-associated virus serotype vectors in 100 healthy Chinese and its potential relation to body constitutions. J. Integr. Med. 13, 341–346.

26. Shen, Y., Li, X., Dong, D., Zhang, B., Xue, Y., and Shang, P. (2018). Transferrin receptor 1 in cancer: a new sight for cancer therapy. Am. J. Cancer Res. 8, 916–931.

27. Shen, Y., Li, X., Zhao, B., Xue, Y., Wang, S., Chen, X., Yang, J., Lv, H., and Shang, P. (2018). Iron metabolism gene expression and prognostic features of hepatocellular carcinoma. J. Cell. Biochem. 119, 9178–9204.

28. Udali, S., Castagna, A., Corbella, M., Ruzzenente, A., Moruzzi, S., Mazzi, F., Campagnaro, T., De Santis, D., Franceschi, A., Pattini, P., et al. (2018). Hepcidin and DNA promoter methylation in hepatocellular carcinoma. Eur. J. Clin. Invest. 48, e12870.

29. Adada, M.M., Canals, D., Jeong, N., Kelkar, A.D., Hernandez-Corbacho, M., Pulkoski-Gross, M.J., Donaldson, J.C., Hannun, Y.A., and Obeid, L.M. (2015). Intracellular sphingosine kinase 2-derived sphingosine-1-phosphate mediates epidermal growth factor-induced ezrin-radixin-moesin phosphorylation and cancer cell invasion. FASEB J. 29, 4654–4669.

30. Díaz, R., Troncoso, J., Jakob, E., and Skugor, S. (2021). "Limiting access to iron decreases infection of Atlantic salmon SHK-1 cells with bacterium Piscirickettsia salmonis". BMC Vet. Res. 17, 155.

31. Cui, J., Guo, X., Li, Q., Song, N., and Xie, J. (2020). Hepcidin-to-Ferritin Ratio Is Decreased in Astrocytes With Extracellular Alpha-Synuclein and Iron Exposure. Front. Cell. Neurosci. 14, 47.

32. Charlebois, E., and Pantopoulos, K. (2021). Iron overload inhibits BMP/SMAD and IL-6/STAT3 signaling to hepcidin in cultured hepatocytes. PLoS ONE 16, e0253475.

33. Pinnix, Z.K., Miller, L.D., Wang, W., D'Agostino, R., Jr., Kute, T., Willingham, M.C., Hatcher, H., Tesfay, L., Sui, G., Di, X., et al. (2010). Ferroportin and iron regulation in breast cancer progression and prognosis. Sci. Transl. Med. 2, 43ra56.

34. Liang, W., Li, Q., and Ferrara, N. (2018). Metastatic growth instructed by neutrophil-derived transferrin. Proc. Natl. Acad. Sci. USA 115, 11060–11065.

35. Furuta, M., Ueno, M., Fujimoto, A., Hayami, S., Yasukawa, S., Kojima, F., Arihiro, K., Kawakami, Y., Wardell, C.P., Shiraishi, Y., et al. (2017). Whole genome sequencing discriminates hepatocellular carcinoma with intrahepatic metastasis from multicentric tumors. J. Hepatol. 66, 363–373.

36. Longo, V., Brunetti, O., D'Oronzo, S., Ostuni, C., Gatti, P., and Silvestris, F. (2014). Bone metastases in hepatocellular carcinoma: an emerging issue. Cancer Metastasis Rev. 33, 333–342.

37. Mody, K., Mansfield, A.S., Vemireddy, L., Nygren, P., Gulbo, J., and Borad, M. (2019). A phase I study of the safety and tolerability of VLX600, an Iron Chelator, in patients with refractory advanced solid tumors. Invest. New Drugs 37, 684–692.

38. Kunos, C.A., Chu, E., Makower, D., Kaubisch, A., Sznol, M., and Ivy, S.P. (2017). Phase I Trial of Triapine-Cisplatin-Paclitaxel Chemotherapy for Advanced Stage or Metastatic Solid Tumor Cancers. Front. Oncol. 7, 62.

39. Tang, Y., Cai, X., Zhang, H., Shen, H., Wang, W., Shen, Z., Gu, W., Ling, C., and Li, M. (2017). miR-212 mediates counter-regulation on CRH expression and HPA axis activity in male mice. J. Mol. Endocrinol. 59, 365–375.

40. Zheng, X., Jiang, T., Wu, H., Zhu, D., Wang, L., Qi, R., Li, M., and Ling, C. (2011). Hepatic iron stores are increased as assessed by magnetic resonance imaging in a Chinese population with altered glucose homeostasis. Am. J. Clin. Nutr. 94, 1012–1019.

41. Zhou, S.L., Hu, Z.Q., Zhou, Z.J., Dai, Z., Wang, Z., Cao, Y., Fan, J., Huang, X.W., and Zhou, J. (2016). miR-28-5p-IL-34-macrophage feedback loop modulates hepatocellular carcinoma metastasis. Hepatology 63, 1560–1575.
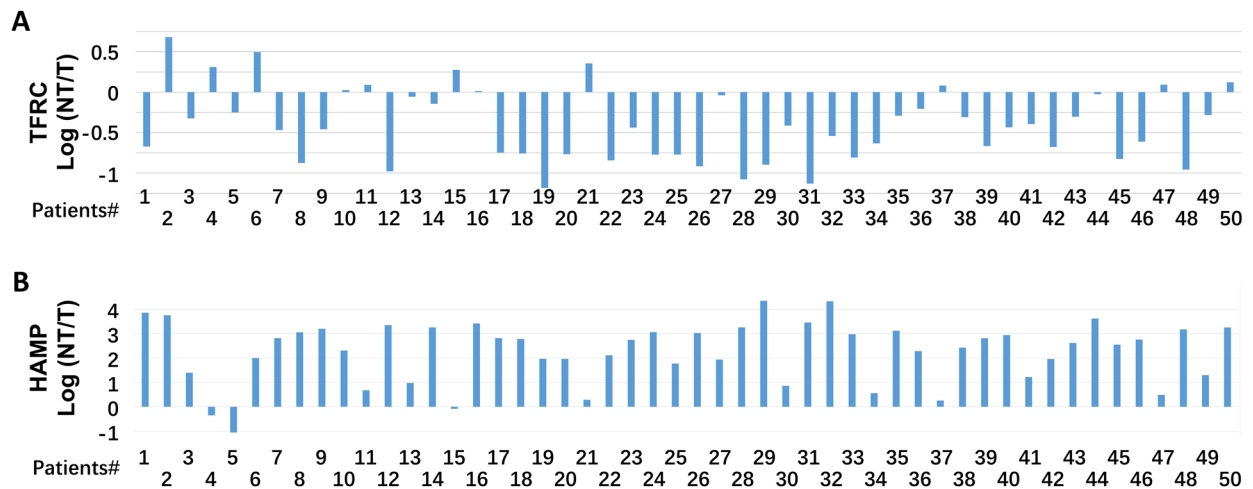
Supplemental Information

Sphingosine-1-phosphate transporter spinster

homolog 2 is essential for iron-regulated

metastasis of hepatocellular carcinoma

Min Li, Yuxiao Tang, Dongyao Wang, Xiaofeng Zhai, Hui Shen, Chen Zhong, Man Yao, Aiguo Jin, Zhengjun Zhou, Shaolai Zhou, Jia Fan, Chang-quan Ling, and Chen Ling

SUPPLEMENTARY FIGURES AND FIGURE LEGENDS

Fig. S1. Most HCC patients showed low iron statues in the HCC samples compared to their non-tumor adjacent samples. Data was retrieved from the public TCGA database (https://portal.gdc.cancer.gov/). The mRNA expression levels of **(A)** TFRC and **(B)** HAMP in the non-tumor (NT) samples were divided by those in the solid tumor (T) samples from the same patient. The log value is presented. HCC: hepatocellular carcinoma; TFRC: transferrin receptor; HAMP: hepcidin.
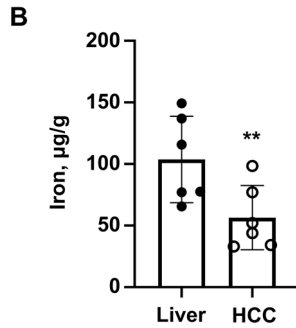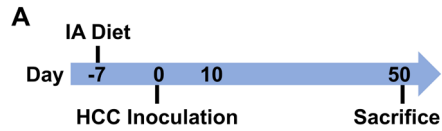
Fig. S2. HCC tumor had less iron than normal liver in an orthotopic mouse model.

(A) C57BL/6 mice were fed with IA diet at Day -7. Mouse HCC H22 cells were orthotopically administrated at Day 0. All mice were sacrificed at Day 50. N=5 **(B)** Iron content in the normal liver and growing HCC was determined.
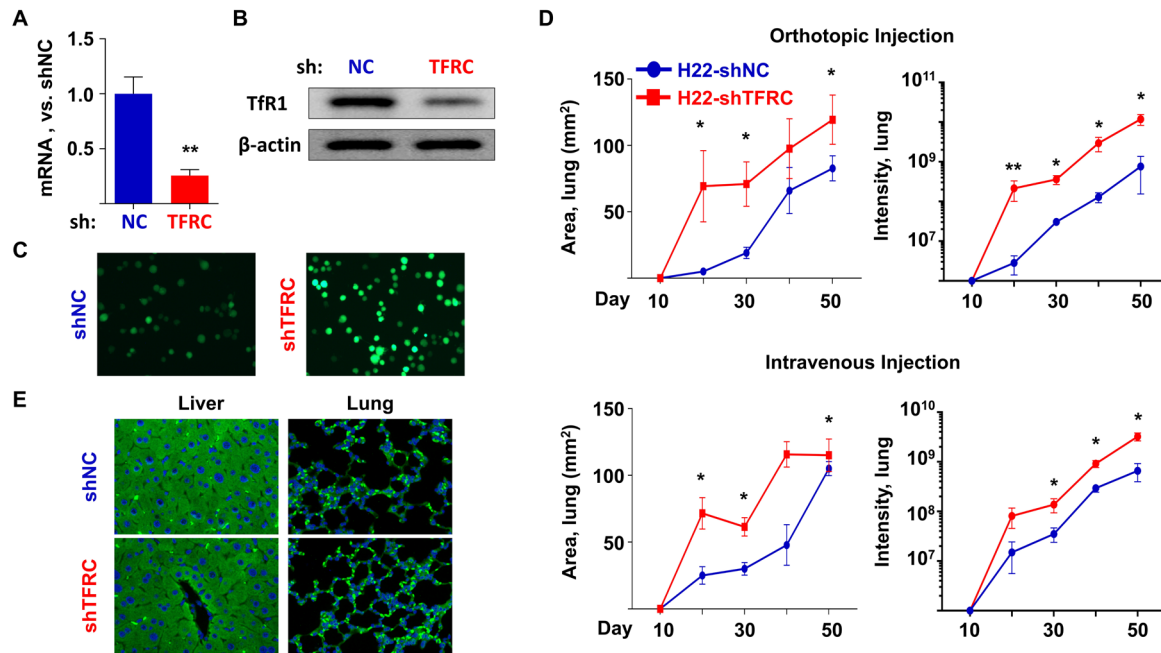
Fig. S3. TFRC-knockdown enhanced H22 cell metastasis *in vivo*.

(A) Quantitative reverse-transcription PCR and **(B)** Western blot assays to validate the knockdown efficiency of lentiviral mediated shTFRC in H22 cells.

(C) Phen Green-FL fluorescence signal quenching assay showed significantly decreased iron accumulation in the TFRC-knockdown H22 cells.

(D to E) C57BL/6 mice were fed with IA diet at Day -7. TFRC-knockdown (shTFRC) mouse HCC H22 cells or their control counterparts (shNC) were orthotopically or intravenously administrated at Day 0. All mice were sacrificed at Day 50. N=3 **(D)** Growth of tumor cells over time in the lung of C57BL/6 mice. **(E)** Fluorescent immunostaining showed ferritin expression in the liver and lung of the tumor-bearing C57BL/6 mice at sacrifice. Data is related to Figure. 2G.

Data was presented as mean $\pm$ SEM. *p < 0.05, **p < 0.01 vs. shNC. HCC: hepatocellular carcinoma; TFRC: transferrin receptor.
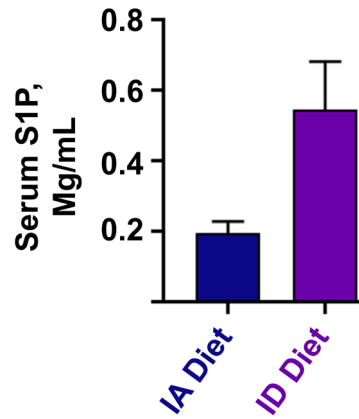
Fig. S4. Iron deficiency induced serum S1P level. C57BL/6 mice were fed with either

IA or ID diet for 2 months. The S1P content in serum was determined by liquid

chromatography‑mass spectrometry (LC-MS).
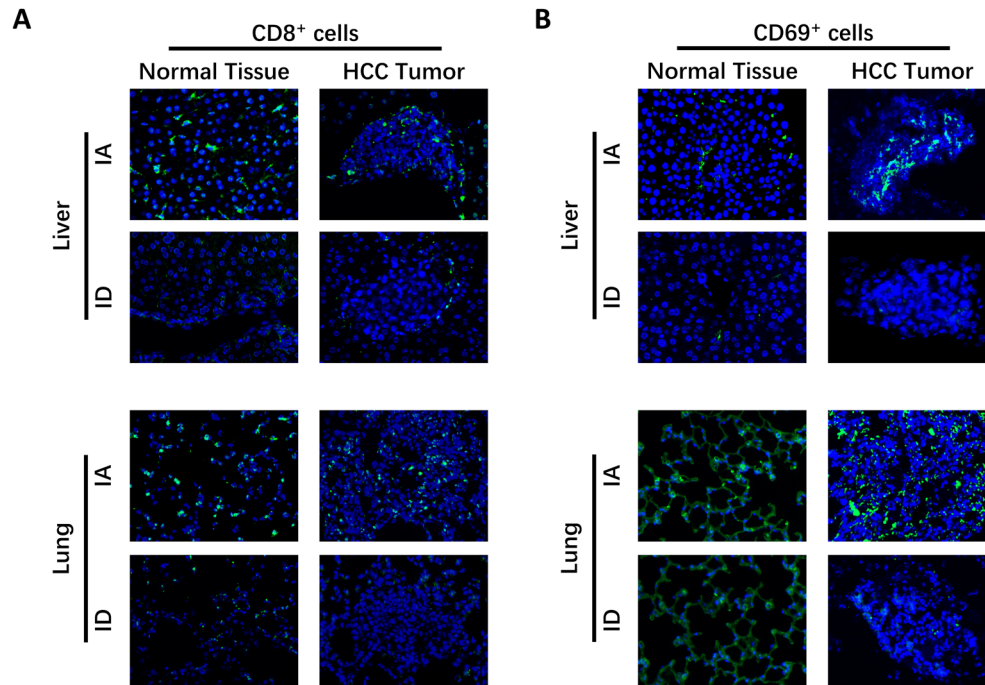
Fig. S5. Iron deficiency reduced CD8+ and CD69+ cells in the tumor-bearing mouse liver and lung. C57BL/6 mice were fed with either IA or ID diet at Day -7. Mouse HCC H22 cells were orthotopically administrated at Day 0. All mice were sacrificed at Day 50. The liver and lung tissues were obtained, followed by immune fluorescent staining against **(A)** CD8 and **(B)** CD69. Data is related to Fig. 3C. N=3.

IA: iron-adequate; ID: iron-deficient; HCC: hepatocellular carcinoma.
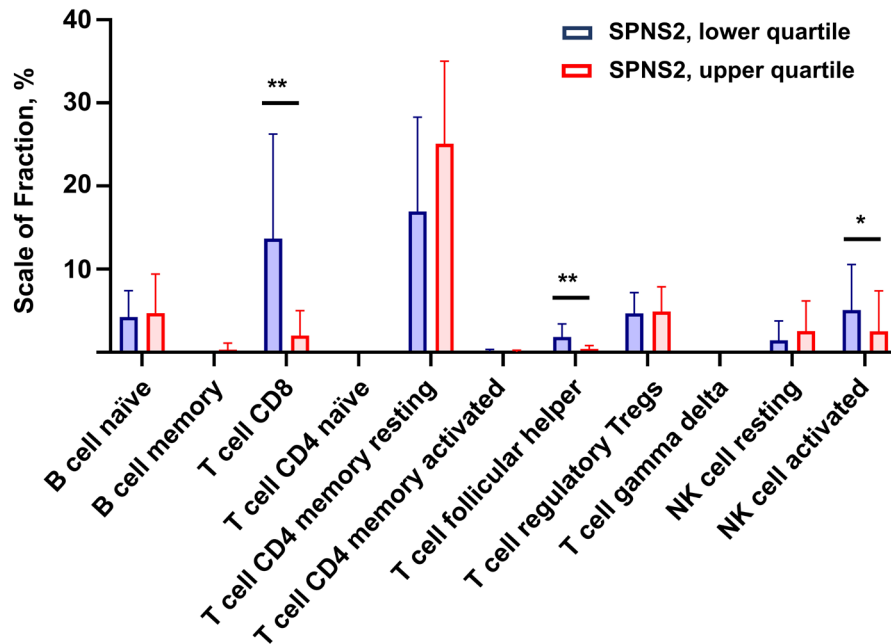
Fig. S6. Comparison of CIBERSORT immune cell fraction between HCC tissues with high and low SPNS2 expression. Gene-expression profiles of HCC tissues were obtained from the TCGA database and patients were divided into two groups based on the lower and upper quartile of transcripts per million values of SPNS2. The data were uploaded to the Cell-type Identification by Estimating Relative Subsets of RNA Transcripts (CIBERSORT) web portal (http://cibersort.stanford.edu/) and were analyzed by the algorithm using the LM22 signature and 1,000 permutations (Nat Methods. 2015;12(5):453-7.). *, P<0.05; **, P<0.05 vs. lower quartile.
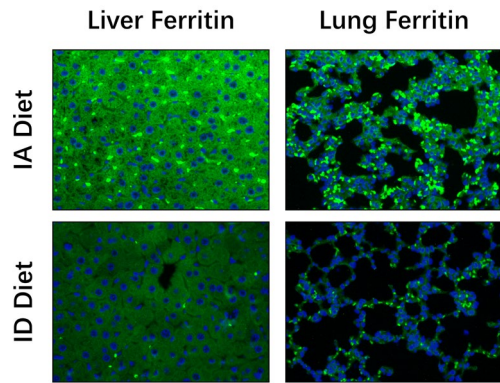
Fig. S7. Characterization of iron deficiency in the tumor-bearing nude mice. Nude mice were fed with either IA or ID diet at Day -7. Human HCC Huh7 cells were orthotopically or intravenously administrated at Day 0. All mice were sacrificed at Day 50. Ferritin expression in the liver and lung were determined by immunofluorescence staining at sacrifice. Data is related to Fig. 4A. N=6.

IA: iron-adequate; ID: iron-deficient; HCC: hepatocellular carcinoma;
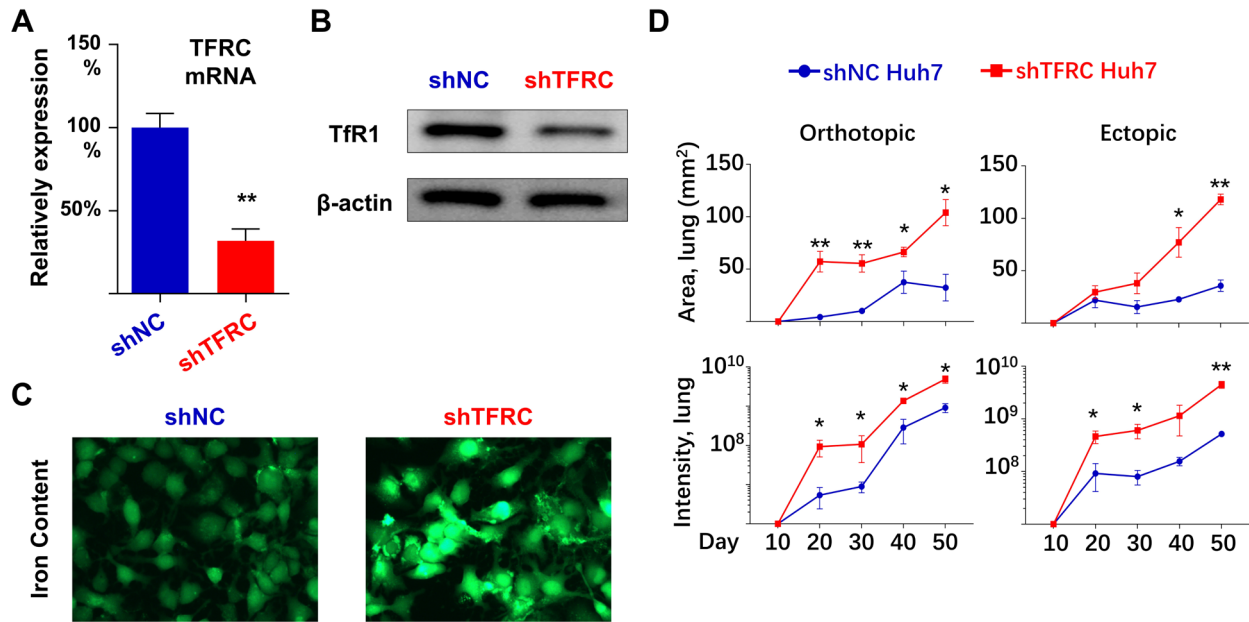
Fig. S8. Characterization of TFRC knockdown in the Huh7 cells. (A) RT-qPCR, **(B)** Western blot and **(C)** Phen Green-FL fluorescence signal quenching assays indicated the reduced TFRC mRNA, TfR1 protein and iron accumulation, respectively. **(D)** Growth of tumor cells over time in the lung of nude mice. Nude mice were fed with IA diet at Day -7. TFRC-knockdown (shTFRC) human HCC Huh7 cells or their negative control counterparts (shNC) were orthotopically or intravenously administrated at Day 0. All mice were sacrificed at Day 50. N=3.

Data was presented as mean $\pm$ SEM. $*p < 0.05$, $**p < 0.01$ vs. shNC. HCC: hepatocellular carcinoma; TFRC: transferrin receptor.
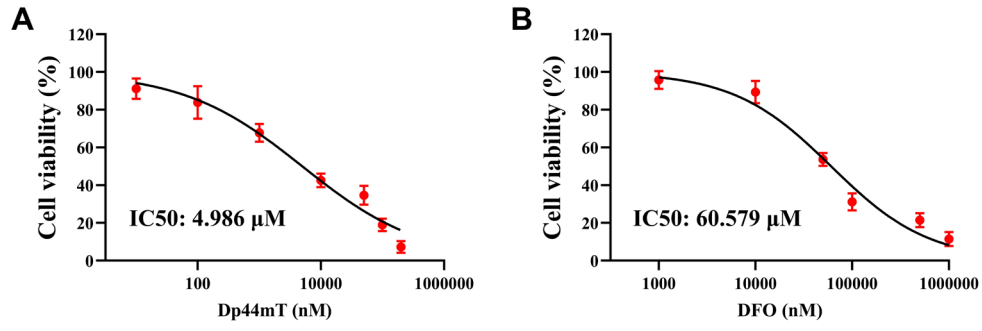
**Fig. S9. The IC50s of Dp44mT and DFO in the Huh7 cells.**
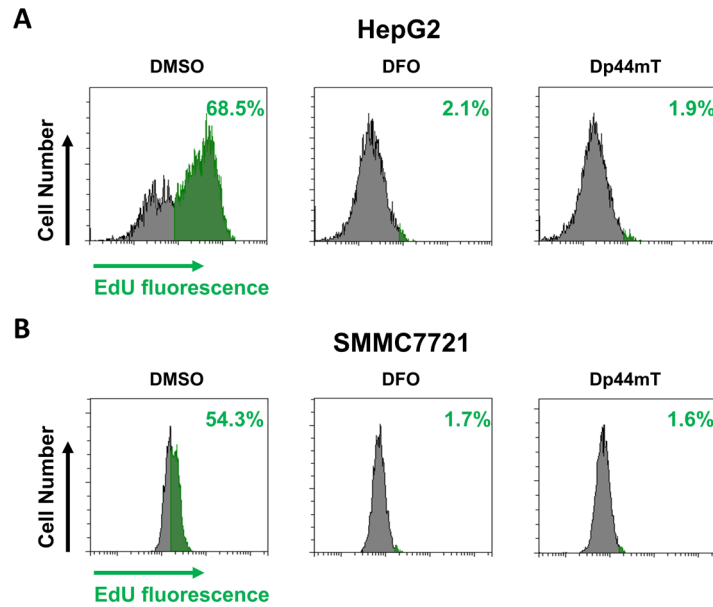
Fig. S10. Iron depletion led to cell growth inhibition of human liver cancer cell lines *in vitro*. Human HCC cell lines **(A)** HepG2 and **(B)** SMMC7721 were treated with either DMSO or iron chelators (DFO and Dp44mT) for 24h. The number of dividing cells were determined by EdU fluorescence levels.

DMSO: dimethyl sulfoxide; DFO: deferoxamine; Edu: 5-Ethynyl-2´-deoxyuridine.
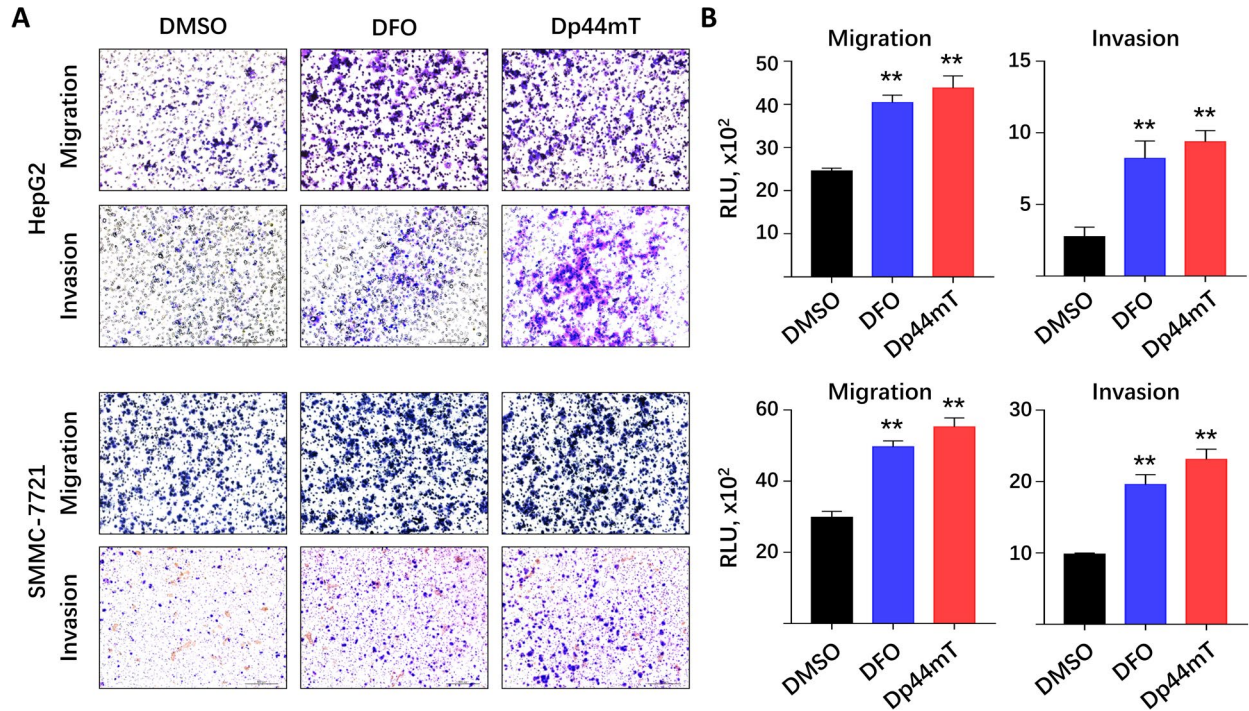
Fig. S11. Iron depletion increased migration and invasion abilities of various human liver cancer cell lines *in vitro*. Human HCC cell lines HepG2 and SMMC7721 were treated with either DMSO or iron chelators (DFO and Dp44mT) for 24h. Both migration and invasion abilities were determined. **(A)** Representative figures and **(B)** quantitative data were showed.

All *in vitro* experiments were performed as 3 replications. Data was presented as mean $\pm$ SEM. *p < 0.05, **p < 0.01 vs. DMSO. HCC: hepatocellular carcinoma; DMSO: dimethyl sulfoxide; DFO: deferoxamine.
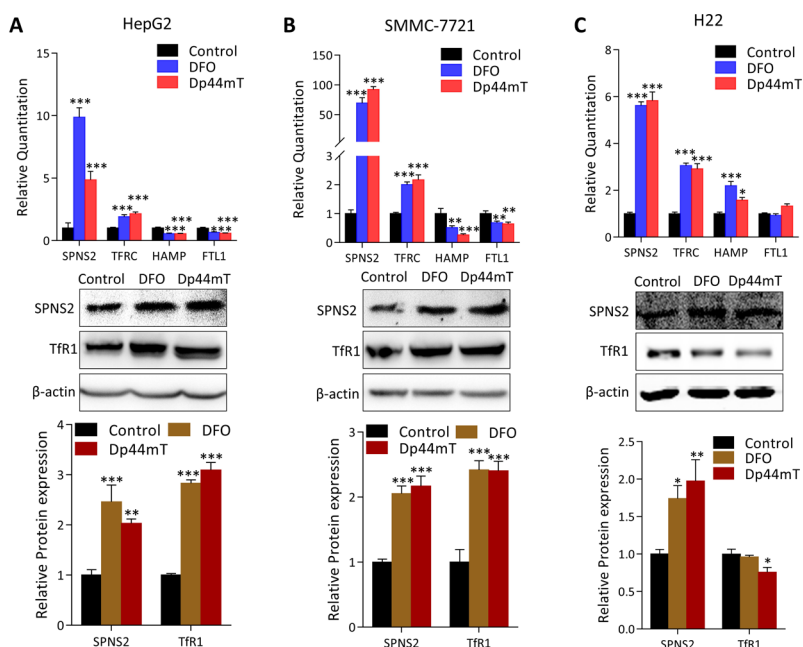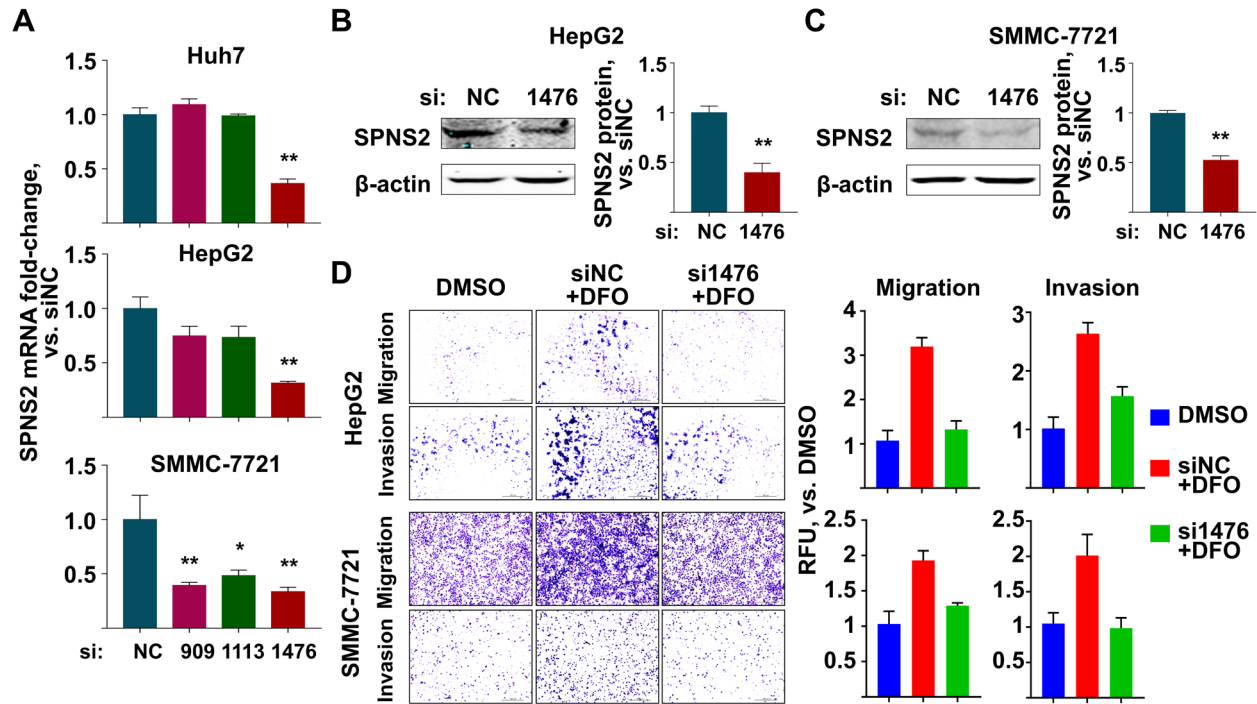
Fig. S12. The mRNA and protein expression of SPNS2 and iron-related genes in various HCC cells *in vitro*, under the treatment of iron depletion. (A) HepG2, **(B)** SMMC-7721, and **(C)** H22 cells were treated with either DMSO or iron chelators (DFO or Dp44mT) for 24h. The mRNA (upper) and protein (lower) expression of SPNS2 and iron-related genes were determined.

All *in vitro* experiments were performed as 3 replications. Data was presented as mean ± SEM. *p < 0.05, **p < 0.01 vs. DMSO. HCC: hepatocellular carcinoma; DMSO: dimethyl sulfoxide; DFO: deferoxamine; SPNS2: transporter spinster homologue 2; TFRC: transferrin receptor; HAMP: hepcidin; FTL: ferritin light chain.

Fig. S13. The protein expression of FTL and validation of the anti-FTL antibody. (A) Huh7 and HepG2 cells were treated with either DMSO control, or Dp44mT for 24 hours . (B) C57BL/6 mice were fed with IA or ID diet for 2 months. Total protein was extracted and Western blot assay was performed against for Ferritin light chain.

Fig. S14. Inhibition of SPNS2 expression rescued the enhancement effect of iron-depletion on the migration and invasion abilities of human HCC cell lines *in vitro*.

(A) Screening the inhibition efficiency of various siRNAs against SPNS2. mRNA expression was determined at 24 hours post-siRNA treatment.

(B and C) Western blot assays indicated the inhibition of SPNS2 expression post-siRNA treatment.

(D) Migration and invasion abilities of HepG2 (upper) and SMMC-7721 cells (lower) after the treatment of siRNA against SPNS2.

All *in vitro* experiments were performed as 3 replications. Data was presented as mean ± SEM. *p < 0.05, **p < 0.01 vs. siNC. HCC: hepatocellular carcinoma; DMSO: dimethyl sulfoxide; DFO: deferoxamine; SPNS2: transporter spinster homologue 2.
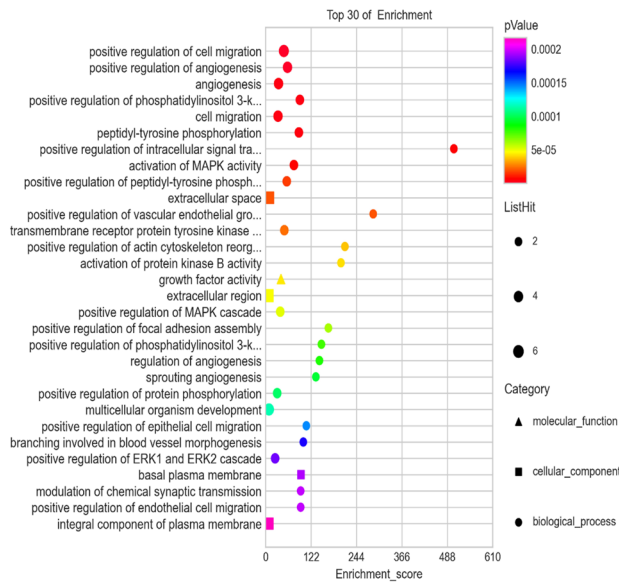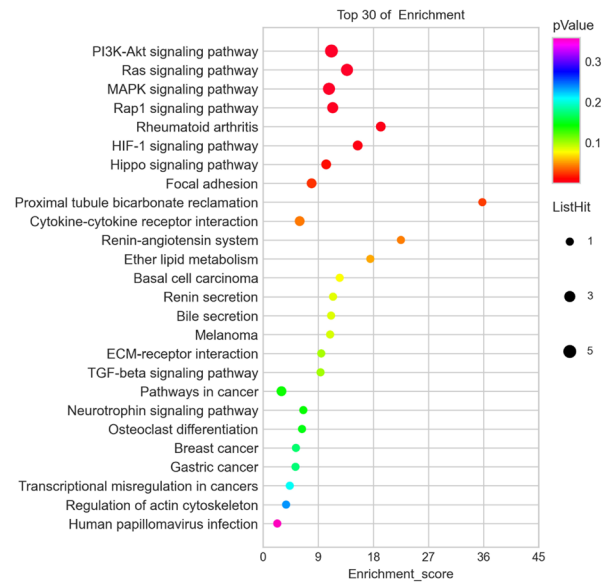
Fig. S15. The GO and KEGG enrichment analysis for metastasis-related genes.

C57BL/6 mice were fed a purified diet with no added iron and separated into ID, IA, and IO groups. Two weeks after iron injection, total hepatic RNA was subjected to Affymetrix GeneChip Mouse Gene 1.0 ST Array analysis. The magnitude of gene counts compared to all the background genes is represented by the horizontal bar length. The significance levels are represented by the legend's color saturation.
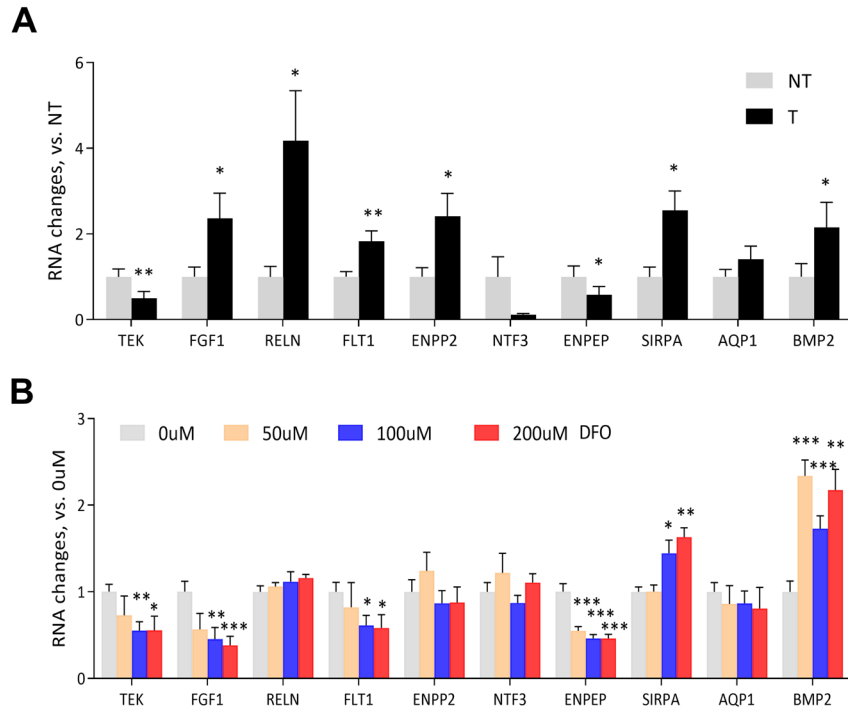
Figure S16. Expressions of metastasis-related genes in iron-deficient cells. Total RNAs were isolated from (A) human liver cancer samples and (B) iron chelator DFO-treated Huh7 cells, followed by qRT-PCR to determine the expression levels of metastasis-related genes. NT, adjacent non-tumor tissue. T, tumor tissue.

Fig. S17. The strategy to generate and identify SPNS2 knockout mice. The knockout of SPNS2 gene was performed by CRISPR /Cas9 system and guided by two gRNAs, as shown in the following figure. This strategy made KO mice loss exon 3, 4, and 5 in the SPNS2 gene. The pairs of PCR primers, F1&R1 and F2&R1, were used to amplify DNA bands for KO and WT mice. The WT band amplified by R1 and F2 equals to 409bp, while the KO band amplified by R1 and F1 equals to 613bp.
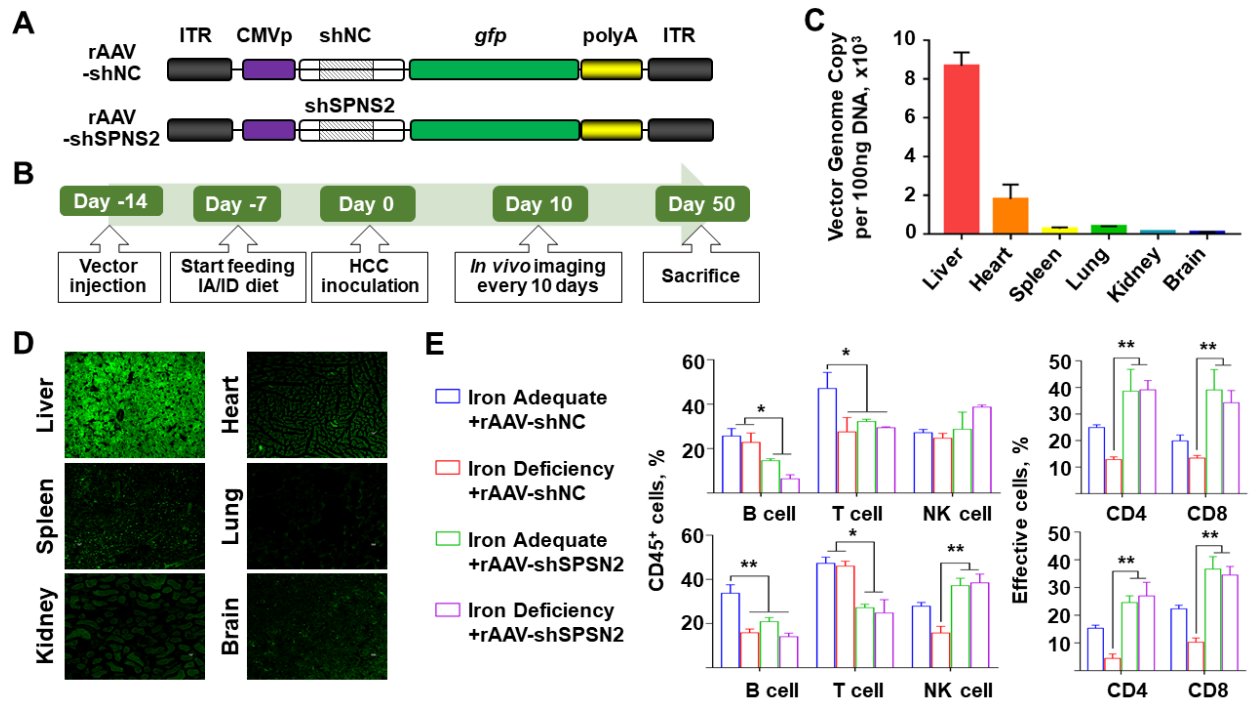
Fig. S18. Validation of recombinant adeno-associated virus (rAAV) serotype 8 vectors *in vivo*.

(A) Schematic genome structures of rAAV vectors containing shNC/shSPNS2 and a green fluorescent protein (*gfp*) gene. Both vectors were under the control of a ubiquitous CMV promoter (CMVp).

(B) Protocols for analysis of HCC metastasis post-viral injection.

(C and D) Non-tumor C57BL/6 mice were tail-vein injected with rAAV vectors. **(C)** The vector genome copy number and **(D)** GFP expression in various mouse tissues at Week 4 post-viral injection. N=3

(E) C57BL/6 mice were tail-vein injected with rAAV vectors at Day -14 and fed with either IA or ID diet at Day -7. Mouse HCC H22 cells were orthotopically administrated at Day 0. All mice were sacrificed at Day 50. The percentage of lymphocyte subsets and

that of effective T cells in the liver (upper) and lung (lower) were determined by flow cytometry assay. Effective: CD 44^{high}, CD62^{Low}. Data is related to Fig 4E. N=3

Data was presented as mean $\pm$ SEM. *p < 0.05, **p < 0.01. IA: iron-adequate; ID: iron-deficient; HCC: hepatocellular carcinoma; SPNS2: transporter spinster homologue 2; ITR: inverted terminal repeat; CMVp: cytomegalovirus promoter.

SUPPLEMENTARY TABLE

Table S1. Sequences of primers for amplification of cDNA.

Name	sequence
hsa18s-F	TAACGAACGAGACTCTGGCAT
hsa18s-R	CGGACATCTAAGGGCATCACAG
hsaTFRC-F	GGGATACCTTTCGTCCCTGC
hsaTFRC-R	ACCGGATGCTTCACATTTTGC
hsaHAMP-F	CTGTTCCCTGTCGCTCTGTT
hsaHAMP-R	AGTTGTCCCGTCTGTTGTGG
hsaFerritin-F	GGACCCCCATCTCTGTGACT
hsaFerritin-R	AGTCGTGCTTGAGAGTGAGC
hsaSPNS2-F	AACGTGCTCAACTACCTGGAC
hsaSPNS2-R	GAAGCTACAGATGAACACTGACTG
mmu-18s-F	GTAACCCGTTGAACCCCATT
mmu-18s-R	CCATCCAATCGGTAGTAGCG
mmuHAMP-F	CAGGGCAGACATTGCGATAC
mmuHAMP-R	GCAACAGATACCACACTGGGA
mmuFerritin-F	GCTCCTTGCCCGGGACTTA
mmuFerritin-R	AAAAAGAAGCCCAGAGAGAGGT

mmuTFRC-F	GGCGCTTCCTAGTACTCCCT
mmuTFRC-R	ATAGCCCAGGTAGCCACTCA
mmuSPNS2-F	TGAAGGCCCTGATCCGAAAC
mmuSPNS2-R	ATGAGGCTGTCTTTGGCTCC

Table S2. Sequences of primers for amplification of genomic DNA.

TFRC-sg-5in-tF	TCTTTCTATATTGCCTCAGGTTGAC
TFRC-sg-3in-tR	GGTGTCAGCAAACTCTATGGAGTTC
SPNS2-F1	AGAATACATGAGACCCTGCGTTTG
SPNS2-F2	CAGAGACCAGGCTTTGACCTTC
SPNS2-R1	CACTTTGTCTTGAGCTTCCGC

Table S3. Sequences for siRNA, shRNA and Cas9 guide RNA.

SPNS2-gRNA-F	ATCCCCAGGGCCGCAGTCCAGGG
SPNS2-gRNA-R	TTACTTACTGCATCACCCCCAGG
Lenti-has-TFRC shRNA	CCGGTTGTATGTTGAAAATCAATTTCGCTCGA GCGAAATTGATTTTCAACATACAAATTTTT
Lenti-mmu-TFRC shRNA	CCGGTGCTAATTTTGGCACTAAAAAGGCTCGA GCCTTTTTAGTGCCAAAATTAGCATTTTT
siSPNS2-909-sense	CCGUCUUCUACUUCGCCAUTT

siSPNS2-909-antisense	AUGGCGAAGUAGAAGACGGTT
siSPNS2-1113-sense	CCUCAUGGCUCCGAGAUAUTT
siSPNS2-1113-antisense	AUAUCUCGGAGCCAUGAGGTT
siSPNS2-1476-sense	GCAUCGUAGGAGCCUAUAUTT
siSPNS2-1476-antisense	AUAUAGGCUCCUACGAUGCTT